Zummo FP, Cullen KS, Honkanen-Scott M, Shaw JAM, Lovat PE, Arden C. Glucagon-like peptide-1 protects pancreatic beta-cells from death by increasing autophagic flux and restoring lysosomal function. *Diabetes* 2017. DOI: 10.2337/db16-1009.

Title:

Glucagon-like peptide-1 protects pancreatic beta-cells from death by increasing autophagic flux and restoring lysosomal function.

Authors:

Francesco P Zummo, Kirsty S Cullen, Minna Honkanen-Scott,

James AM Shaw, Penny E Lovat, Catherine Arden*.

Author Affiliation:

Institute of Cellular Medicine, Newcastle University, Newcastle-upon-Tyne, UK

*** Corresponding Author**

Dr Catherine Arden, Institute of Cellular Medicine, Newcastle University, 4th Floor William Leech Building, Medical School, Newcastle-upon-Tyne, NE2 4HH, UK. Tel: 0191 2088798.

Email: Catherine.Arden@ncl.ac.uk

Running title:

GLP-1 restores autophagic flux in beta-cells

Word count: 4000

Number of Figures and Tables: 8 Figures, 0 Tables

Number of Online Supplemental Material: 2 Tables, 3 Figures, 1 Video

Abbreviations:

Atg5, autophagy related protein 5; BECN1, Beclin 1; CHOP / GADD153, CCAAT-enhancer-binding protein homologous protein; CQ, chloroquine; eIF2α, eukaryotic initiation factor 2; ER stress, endoplasmic reticulum stress; Ex-4, exendin-4; GAPDH, Glyceraldehyde 3-phosphate dehydrogenase; GFP, green fluorescent protein; GLP-1**,** glucagon-like peptide-1; GLT, glucolipotoxicity; JNK, jun n-terminal kinase; Lamp2, lysosome-associated membrane protein 2; LC3, microtubule associated protein 1, light chain 3; LMP, lysosomal membrane permeabilisation; 3-MA, 3-methyladenine; MCOLN1, mucolipin 1; N/C ratio; nuclear: cytoplasmic ratio; PI, propidium iodide; TFEB, transcription factor EB; TUDCA, tauroursodeoxycholic acid; UVRAG, UV radiation resistance-associated gene.

Abstract:

Studies in animal models of type 2 diabetes have shown that glucagon-like peptide-1 (GLP-1) receptor agonists prevent β-cell loss. Whether GLP-1 mediates β-cell survival via the key lysosomal-mediated process of autophagy is unknown.

Here we report that treatment of INS-1E β-cells and primary islets with glucolipotoxicity (0.5mmol/l palmitate, 25mmol/l glucose) increases LC3 II, a marker of autophagy. Further analysis indicates a blockage in autophagic flux associated with lysosomal dysfunction. Accumulation of defective lysosomes leads to lysosomal membrane permeabilisation (LMP) and release of Cathepsin D, which contributes to cell death. Our data further demonstrated defects in autophagic flux and lysosomal staining in human samples of type 2 diabetes. Co-treatment with the GLP-1 receptor agonist exendin-4 reversed the lysosomal dysfunction, relieving the impairment in autophagic flux and further stimulated autophagy. siRNA knockdown showed the restoration of autophagic flux is also essential for the protective effects of exendin-4.

Collectively, our data highlights lysosomal dysfunction as a critical mediator of β-cell loss and shows that exendin-4 improves cell survival via restoration of lysosomal function and autophagic flux. Modulation of autophagy / lysosomal homeostasis may thus define a novel therapeutic strategy for type 2 diabetes, with the GLP-1 signalling pathway as a potential focus.

Macroautophagy (hereafter referred to as autophagy) is the principle lysosomal mediated mechanism for the degradation of misfolded proteins and damaged organelles to sustain intracellular homeostasis and core metabolic functions (1). Cytosolic components are engulfed by autophagosomes which fuse with lysosomes to allow for degradation of contents by lysosomal hydrolases. This process generates amino acids, lipids and nucleotides for biosynthesis or for use as energy sources during starvation and can also serve to remove superfluous nutrients in metabolically active tissues. Under most conditions, autophagy acts to prevent or delay cell death, but can result in cell death through deregulation or exacerbation. Lysosomal function and fusion with autophagosomes are critical mediators of autophagic flux and its pro-survival vs. pro-death role (1-3).

Recent studies have implicated a role for β-cell autophagy in the development of type 2 diabetes (4). The overt β-cell failure evident in type 2 diabetes (5) is a consequence of both deterioration of function and loss of cell mass (6) and is in part attributed to the cytotoxic effects of chronically elevated glucose and fatty acids (glucolipotoxicity) (7). The impact of gluco-/lipo-toxicity on β-cell autophagy has been proposed to be both beneficial and detrimental to cell survival. Autophagy-deficient β-cells show compromised function and survival upon high-fat feeding supporting a protective role for autophagy (8), a finding supported by *in vitro* studies of gluco-/lipo-toxicity (9-13. In contrast, other studies report that chronic lipotoxicity causes defective autophagic turnover leading to cell death (14-16), consistent with increased autophagosome accumulation in human and rodent type 2 diabetes (17-18). Such studies have suggested that the impairment in autophagic flux may be secondary to defects in lysosomal function (14, 16) but the underlying mechanisms have not been elucidated and the impact of this defect on lysosomal-mediated cell death has not been explored.

Glucagon Like Peptide-1 (GLP-1) receptor agonists lower blood glucose through distinct actions on various organs including β-cells (19). GLP-1 agonists enhance insulin secretory capacity by increasing glucose-induced insulin secretion and by preserving β-cell mass by stimulation of β-cell proliferation and inhibition of cell death (20). Studies in other tissues, including liver and spinal cord, have shown that GLP-1 agonists activate autophagy and that this mechanism is essential for the cell survival effects of the drug (21, 22). However, the precise role of GLP-1 in regulating β-cell autophagy and its impact on cell fate has not been defined. To this aim we have explored the role for autophagy in the pro-survival effects of GLP-1 in β-cells exposed to glucolipotoxicity. The results provide a mechanistic insight into the deregulation of autophagy and lysosomal dysfunction in pancreatic β-cells exposed to excess nutrients and identify restoration of these pathways as critical components for the pro-survival effect of the GLP-1 receptor agonist exendin-4.

Research Design and Methods

Rodent Islet isolation

8-10 week old C57BL/6 mice fed *ad libitum* were euthanised by cervical dislocation. All procedures conformed to Home Office Regulations and approved by Newcastle University Ethical Committee. Pancreases were perfused with collagenase-P via the common bile duct and islets purified using a Histopaque gradient (23) with a final filtration step using a 70 μm filter. Islets were cultured overnight in RPMI-1640 supplemented with 10% FBS and 50 U/ml penicillin and 50 μg/ml streptomycin prior to treatment.

Human Islets

Human islets were isolated from 7 non-diabetic donors at the Clinical Islet Lab, University of Alberta, Canada or the Islet Isolation Unit, Kings College London, UK with appropriate ethical approval. Islets were transported to Newcastle and maintained in CMRL media supplemented with 0.5% human albumin serum and 50 U/ml penicillin and 50 μg/ml streptomycin for 24 h prior to treatment.

Immunohistochemical analysis of human tissue

Pancreatic tissue / islets from 8 donors (3 type 2 diabetic: age, 59.0±6.6 years; BMI, 26.8±4.3 kg/m^2; metformin: 2 patients; 5 non-diabetic: age, 42.9±14.2 years; BMI, 27.1±4.1 kg/m^2) were studied. Ethical approval was acquired from Newcastle and North Tyneside ethics committee and research consent obtained. Following fixation in formalin and embedding in paraffin, indirect immunofluorescence staining was carried out as in (24). Tissue was imaged using a Zeiss Axio Imager II microscope and a minimum of five islets from one section was imaged per patient. The p62 signal intensity of the islets was quantified using ImageJ and non-islet staining subtracted. Data is expressed as p62 intensity/islet.

Cell culture

INS-1E cells were cultured in RPMI-1640 media containing 50 μmol/l β-mercaptoethanol, 1 mmol/l sodium pyruvate, 50 U/ml penicillin, 50 μg/ml streptomycin and 5% FBS. Palmitate:BSA was prepared as in (11). For Atg5 silencing, INS-1E cells were transfected with scrambled siRNA or siRNA targeted against Atg5 for 48 h using Lipofectamine® RNAiMAX (Thermo Fisher, Loughborough, UK) according to the manufacturer's instructions.

INS-1E(mCherry-GFP-LC3) model

INS-1E cells were transfected with pBABE-puro mCherry-EGFP-LC3B (a gift from Jayanta Debnath (25) (Addgene plasmid # 22418)) and cells selected using 1 μg/ml puromycin. INS-1E (mCherry-GFP-LC3) cells were plated on chambered coverslips and nuclei stained with 4.5 μg/ml Hoechst for 5 min. Live cell imaging was performed in a heated environmental chamber (37°C, 5% CO_2) using either a Nikon TE2000 (×100) or using a Nikon AIR (x100). Images were processed using NIS Element Imaging software and puncta quantified using Volocity.

INS-1E(GFP-LC3) model

INS-1E cells were transfected with EGFP-LC3 (26) (a gift from Karla Kirkegaard (Addgene plasmid #11546)) and cells selected using 1 μg/ml puromycin. INS-1E(GFP-LC3) were plated onto coverslips and co-stained with 75 nmol/l lysotracker Red DND-99 (ThermoFisher) for 30 min before fixation with 4% paraformaldehyde. Nuclei were stained with 4.5 μg/ml Hoechst 33342 and coverslips mounted onto slides. Cells were imaged using a Nikon Eclipse E400 (x60). Co-localisation between GFP-LC3 and lysosomes was visually quantified as the number of GFP-LC3 puncta co-staining for lysotracker. This analysis was performed by two independent observers, one unaware of sample identity.

Cell death measurements

For PI/Hoechst staining, INS-1E / human islets ~~cells~~ were incubated with 10 μg/ml propidium iodide and 10 μg/ml Hoechst-33342 for 20 min. Images were taken with a Nikon TE2000 (×20). For INS-1E, >1000 cells were counted per condition and analysis performed using ImageJ software. For human islets, a minimum of ten islets were analysed and % viability estimated visually by two independent observers, one unaware of sample identity.

Apoptosis was determined using the Caspase-Glo® 3/7 Assay (Promega, Southampton, UK) or by western blotting for cleaved caspase 3.

Western blotting

Proteins were fractionated using 4-12% SDS/PAGE gels (Bio-rad, Hertfordshire, UK) and transferred to PVDF. Membranes were probed with primary antibody (Table S1) at 4°C overnight. After incubation with secondary antibody conjugated to horseradish peroxidase, bands were detected using enhanced chemiluminescence. Immunoblots were quantified using ImageJ.

Immunostaining

Cells plated onto coverslips were fixed with 4% paraformaldehyde and immunostaining performed as in (27). Cells were imaged using a Nikon TE2000 (×100). Lysosomal puncta were quantified using Blobfinder software (Uppsala University, Sweden). TFEB translocation was quantified by measurement of the mean pixel intensity for the nuclear and cytoplasmic compartments using ImageJ and the nuclear:cytoplasmic ratio calculated.

Cathepsin activity assays

For cathepsin activity, INS-1E plated in 24-well plates were extracted into 200 µl cell lysis buffer and Cathepsin B / D detected according to the manufacturer's instructions (Merck Millipore (CBA001) and RayBiotech, Norcross, USA (68AT-CathD-S100), respectively).

RNA extraction and RT-PCR

RNA was extracted using TRIzol (Thermo Fisher) and cDNA was synthesized from 1 µg of RNA with MMLV (Promega). Real-time RT-PCR was performed as in (28) using custom

designed primers (Table S1). Relative mRNA levels were calculated by delta cycle threshold, corrected for cyclophilin A and are expressed relative to control.

Subcellular Fractionation

For analysis of TFEB translocation, nuclear and cytosolic extracts were prepared as in (29). For analysis of lysosomal membrane permeabilisation, cytosolic extracts were prepared as in (30).

Statistics

Results are expressed as means ± SEM for the number of cell preparations and values compared using either the Student's *t*-test (paired or unpaired) or by one or two-way ANOVA followed by Bonferroni's test.

Results

Exendin-4 increases autophagic flux in β-cells exposed to glucolipotoxicity

We first confirmed the protective effects of the GLP-1 agonist exendin-4 over β-cell death. Treatment of INS-1E with glucolipotoxicity (25 mmol/l glucose and 0.5 mmol/l palmitate, (GLT)) increased cell death (Figure 1A) and apoptosis (Figure 1B), which were partially prevented by co-treatment with 100 nmol/l exendin-4 (Figure 1A and B). GLT also increased cell death and apoptosis in human islets and exendin-4 partially prevented this (Figure 1C-E). GLT increased basal autophagic activity, as evidenced by increased LC3 II in INS-1E and in mouse and human islets (Figure 1F-H). Exendin-4 had no effect in the absence of GLT but exacerbated the GLT-induced increase in LC3 II (Figure 1F-H).

To investigate autophagic flux, we evaluated LC3 II in the presence of the lysosomal inhibitor chloroquine (31). As expected, chloroquine increased LC3 II (Figure 2A). GLT

continued to increase LC3 II in the presence of chloroquine suggesting autophagic stimulation. However, the effect of GLT was greater in the absence of chloroquine than in its presence (GLT w/o chloroquine 4.8-fold -/+ 0.23 increase, vs. GLT + chloroquine 2.2-fold -/+ 0.46 increase in LC3II/GAPDH, $p<0.005$), suggesting partial blockage of autophagic flux. To further explore this, we used two more robust methods to assess autophagic flux, mCherry-GFP-LC3 analysis and p62 accumulation (31). We first generated INS-1E stably expressing mCherry-GFP-LC3 (32). Validation of this system confirmed that blockage of autophagic flux with chloroquine caused accumulation of yellow puncta (Figure 2B). Exposure of INS-1E(mCherry-GFP-LC3) to GLT also increased yellow puncta (Figure 2C) indicating impairment in flux, whilst treatment with exendin-4 decreased the number of yellow puncta (Figure 2C) indicating restoration of flux. These observations were further supported by observations of GLT-induced p62 accumulation (Figure 2D), consistent with the increase in p62 in tissues from type 2 diabetic patients (Figure 2E) indicating impaired autophagic flux (30). Co-treatment of INS-1E with exendin-4 decreased p62 accumulation (Figure 2D). Collectively, these data demonstrate that the GLT-induced increase in LC3 II represents both autophagic stimulation but also an impairment in flux. Co-treatment with exendin-4 prevents the impairment in autophagic flux and further stimulates autophagy.

Autophagy contributes to the pro-survival effects of Exendin-4

To determine whether autophagy contributes to the pro-survival effects of exendin-4, we first explored the impact of impaired autophagic flux on cell survival. Live-cell imaging of INS-1E(mCherry-GFP-LC3) treated with GLT showed that cells with apparent autophagic dysfunction as evident by large yellow puncta (at 4-6 h), showed evidence of cell death (cell rounding, detachment, loss of fluorescence) at later time-points (indicated by arrows in Figure 3A, Video S1). Further assessment using siRNA knockdown of the key autophagic

gene Atg5 showed that silencing of Atg5 (Figure 3B) partially prevented the exendin-4 induced increase in LC3 II (Figure 3B, C). Silencing of autophagy did not prevent the GLT-induced increase in cell death but did reverse the protective effect of exendin-4, as evidenced by the increase in PI staining (Figure 3D). The impact of exendin-4 on autophagy is therefore essential for its protective role on β-cell survival.

Exendin-4 prevents the glucolipotoxicity-induced impairment in lysosomal function

The mechanism/s for the impairment in autophagic flux in response to GLT are not well understood although a role for lysosomal dysfunction has been proposed (14, 16). To understand how exendin-4 prevents the deregulation of autophagic flux, lysosomal function was assessed. Treatment of INS-1E with GLT decreased lysosomal staining as determined using lysotracker dye and immunostaining for Lamp2, which was partially prevented by co-treatment with exendin-4 (Figure 4A and B). GLT also decreased cathepsin B activity and exendin-4 reversed this (Figure 4C). These effects were not due to changes in protein expression (Figure S1A and B). The decrease in lysosomal staining was accompanied by an increase in lysosomal vesicle size, an effect partially reversed by co-treatment with exendin-4 (Figure 4D). To assess whether the enlarged vesicles represent lysosomes or autolysosomes, lysosomes were stained with lysotracker and autophagosome with GFP-LC3 and the accumulation of these vesicles monitored upon treatment with GLT for 4-8 h. After 4 h treatment, GFP-LC3-containing autophagosomes increased (Figure 4E). Co-localisation of lysosomal puncta (red) with autophagosomes (green) increased after 4h treatment with GLT but decreased at later time points (Figure 4E-F), suggesting loss of autophagosome-lysosomal fusion. Cotreatment with exendin-4 maintained co-localisation between lysosomes and autophasosomes, consistent with restored autophagic flux (Figure 4E-F).

Glucolipotoxicity stimulates lysosomal biogenesis via TFEB translocation

To determine whether the changes in lysosomal function could be explained by alterations in lysosomal biogenesis, we investigated the regulation of transcription factor EB (TFEB). TFEB upregulates expression of genes involved in lysosomal biogenesis and function, autophagosome biogenesis and autophagosome-lysosome fusion (33-34). Inactive in the cytoplasm under basal conditions, TFEB translocates to the nucleus and activates gene transcription upon stimulation with starvation or lysosomal stress (34). Immunostaining for endogenous TFEB showed that under basal conditions, TFEB localised to the cytoplasm (Figure 5A). Treatment with GLT caused translocation of TFEB to the nucleus (Figure 5A), quantified as a 2-fold increase in the nuclear:cytoplasmic (N/C) ratio (Figure 5B). Further analysis using subcellular fractionation confirmed the nuclear translocation of TFEB (Figure 5C). Real-time PCR analysis confirmed increased mRNA expression of a number of TFEB downstream targets including TFEB, MCOLN1, BECN1 and UVRAG (Figure 5D), confirming that GLT promotes lysosomal / autophagosomal biogenesis. Co-stimulation with exendin-4 further exacerbated the GLT-induced translocation of TFEB as determined by the N/C ratio (Figure 5A and B), subcellular fractionation (Figure 5C) and also increased downstream gene transcription (Figure 5D), suggesting that upregulation of lysosomal / autophagosomal biogenesis may contribute to the beneficial effects of exendin-4.

Glucolipotoxicity induces cell death via lysosomal membrane permeabilisation

The accumulation of defective lysosomes with their high concentration of hydrolytic enzymes is potentially hazardous for the cell. Release of these components into the cytoplasm via lysosomal membrane permeabilisation (LMP) can initiate cell death (35). To determine whether the accumulation of defective lysosomes directly contributes to β-cell death, LMP was investigated. Staining of INS-1E for cathepsin B and D showed loss of punctate staining

following treatment with GLT, which was prevented by co-treatment with exendin-4 (Figure 6A and B). Such a staining pattern in the absence of changes in protein expression (Figure S1B and C) can be indicative of LMP. Further assessment by isolation of cytoplasmic fractions showed that exposure to GLT caused release of cathepsin D into the cytoplasm, which was prevented by co-treatment with exendin-4 (Figure 6C). The impact of LMP on total cell death was assessed using cathepsin inhibitors. Co-treatment with antipain, a non-specific inhibitor, partially prevented the GLT-induced increase in β-cell death (Figure 6D). Further analysis using specific inhibitors of cathepsin B (CBi, CA-074) and cathepsin D (CDi, PepstatinA) (Figure S1D and E) showed that whilst CBi had no effect (Figure 6E), CDi prevented the GLT-induced increase in cell death (Figure 6F). This was confirmed in murine islets where CDi partially reversed the GLT-induced increase in apoptosis (Figure 6G), supporting a role for cathepsin D in LMP-induced cell death.

To further explore this mechanism, tissue samples from control and type 2 diabetic patients were stained for cathepsin D. When compared to controls, diabetic tissue showed decreased staining of cathepsin D in insulin positive cells (Figure 6H, Figure S2). Whilst a decrease in cathepsin D expression cannot be excluded, higher magnification images (Figure 6I) indicate loss of punctate staining, similar to that displayed in GLT-treated INS-1E.

Defect in lysosomal function is downstream of ER stress

To elucidate the mechanisms underlying GLT-induced lysosomal dysfunction and its reversal by exendin-4, we investigated whether the lysosomal dysfunction was dependent on autophagy. Autophagy was chemically modulated using 3-methyladenine (3-MA). Despite inhibition of LC3 II formation in response to GLT (Figure 7A), there was no effect of 3-MA on the GLT-dependent decrease in lysosomal staining or its reversal by exendin-4 (Figure 7B), suggesting that these changes are independent of autophagy.

Endoplasmic reticulum (ER) stress is a major driver in GLT-induced cell death (36). To determine whether ER stress also plays a role in GLT-induced lysosomal dysfunction, ER stress was assessed. GLT increased ER stress as evident by an increase in p-eIF2a and CHOP (Figures 7C and D). Blockage of ER stress with the inhibitor tauroursodeoxycholic acid (TUDCA) (Figure 7E), partially prevented the increase in LC3 II induced by GLT (Figure 7F) and also prevented the decrease in lysosomal staining (Figure 7G), and the GLT-induced increase in cell death (Figure 7H). This data supports a model by which ER stress stimulates autophagy but also impairs lysosomal function, preventing fusion of lysosomes with autophagosomes leading to blockage of autophagic flux. Consistent with previous studies (37-38), the GLT-induced increase in ER stress was attenuated by co-incubation with exendin-4 (Figure 7I). This attenuation of ER stress by exendin-4 may underlie the improvement in lysosomal function.

JNK mediates glucolipotoxicity-induced autophagy but not lysosomal dysfunction

We next sought to elucidate the signalling pathways linking ER stress with autophagy and lysosomal dysfunction. Previous studies have linked ER stress to autophagy via JNK signalling (39) but whether JNK regulates lysosomal function is unknown.

GLT increased JNK phosphorylation (Figure 7J). Inhibition of JNK-P using SP600125 prevented the GLT-induced increase in LC3 II (Figure 7J and K), but not GLT-induced decrease in lysosomal staining (Figure 7L). This data shows that whilst JNK signalling mediates the downstream ER stress mechanisms linking to autophagy, it does not mediate the lysosomal dysfunction induced by GLT. There was no effect of exendin-4 on JNK phosphorylation, and JNK inhibition did not prevent exendin-4 induced LC3 II nor attenuation of lysosomal dysfunction (Figures 7J, K and L), suggesting that exendin-4 does not mediate its protective effects via JNK.

Discussion

GLP-1 agonists improve β-cell function and increase β-cell mass through upregulation of proliferation and inhibition of cell death (19-20) although the underlying mechanisms remain unknown. In the current study we have shown that regulation of autophagic flux is a critical component in the pro-survival effects of exendin-4. Our data supports a model where glucolipotoxicity (GLT) induces lysosomal dysfunction leading to deregulation of autophagy and resulting lysosomal cell death. Treatment with exendin-4 reverses the lysosomal dysfunction, relieving the impairment in autophagic flux and improves cell survival by stimulating autophagy.

Whether the regulation of β-cell autophagy by gluco- / lipo-toxicity represents a pro-survival or pro-death mechanism is contentious (8-18). Some studies support a protective role for autophagy in regulating β-cell mass in response to excess nutrients (8-13), whilst others suggest that these stimuli impair autophagic flux leading to cell death (14-18). Our data shows that GLT stimulates β-cell autophagy but that it also impairs flux through the induction of lysosomal dysfunction as indicated by decreased lysosomal staining and decreased cathepsin activity, consistent with previous models of β-cell lipotoxicity (14, 16). This does not appear to be due to an impairment in lysosomal biogenesis, since GLT causes nuclear translocation of TFEB and upregulation of downstream gene transcription. The enlarged lysosomal vesicles are distinct from the accumulated autophagosomes as evident from the loss of overlap between lysosomal stains and autophagosomal GFP-LC3, indicating loss of lysosomal-autophagosomal fusion at later time points. Chemical inhibition of autophagy and ER stress show that the defect in lysosomal dysfunction is independent from autophagy but downstream of the GLT-induced increase in ER stress. ER stress also appears

to be a major driver in the increase in autophagic signalling, consistent with a previous study (39). However, further analysis indicate differing downstream pathways regulating autophagy and lysosomal dysfunction, JNK dependent and independent, respectively. These findings support a model whereby GLT induces ER stress which both stimulates autophagy and induces lysosomal dysfunction. We predict that the increased activation of autophagy in the presence of impaired lysosomal fusion leads to deregulation of autophagic flux and accumulation of autophagosomal and lysosomal vesicles (Figure 8).

The accumulation of autophagic vesicles in tissue from type 2 diabetic patients by both p62 accumulation (current study and 17) and ultrastructure analysis (18), suggests that the impairment in autophagic flux may contribute to the loss of β-cell mass in type 2 diabetes. This hypothesis is supported by our mCherry-GFP-LC3 data showing that following exposure to GLT, cells with impaired autophagic flux appear to undergo cell death at later time points, unlike cells with normal flux which are more likely to survive. Furthermore, the improvement in β-cell survival induced by exendin-4 was dependent on restoration of autophagic signalling. This is similar to that reported for the autophagy activators rapamycin and carbamazepine, which improved β-cell survival under lipotoxic conditions (11, 13, 15). Studies in other cell types have shown that an impairment in autophagic flux can lead to cell death via apoptosis, non-apoptotic mechanisms and also via lysosomal-mediated cell death (35). Alterations in lysosomal enzymes / protein expression has been reported in both human and rodent type 2 diabetes (18, 40) but their contribution to cell death has not been explored. The current study provides strong evidence that the defect in lysosomal function contributes directly to cell death via lysosomal membrane permeabilisation (LMP) (Figure 8). Loss of punctate cathepsin staining without alterations in protein expression suggest release of cathepsin from the lysosomes, a finding supported by detection of cathepsin D in cytoplasmic

fractions. This loss in staining pattern was also evident in tissue from type 2 diabetic patients compared to controls, although a decrease in cathepsin D protein expression cannot be excluded. Treatment with various cathepsin inhibitors indicate that release of cathepsin D from these cells appears to drive GLT-induced cell death. These findings are consistent with recent studies showing lysosomal dysfunction and LMP in the renal tubule and neuronal cortex when exposed to elevated lipid concentrations (41-42). The finding that human type 2 diabetic tissue shows defects in both autophagic flux (p62 accumulation) and lysosomal function (cathepsin D staining) strongly supports a role for lysosomal / autophagic induced cell death as major driver of β-cell death and dysfunction in type 2 diabetes.

GLP-1 agonists improve the insulin secretory response by increasing β-cell mass in animal models of type 2 diabetes, which is due, in part, to a decrease in β-cell death (19-20). Previous studies investigating the impact of GLP-1 agonists on β-cell autophagy have shown that GLP-1 increases LC3 II levels and autophagosomal formation in conditions of high fat diet / lipotoxicity (43-44) but that it inhibits autophagic stimulation in a model of tacrolimus-induced diabetes (45). Through the rigorous assessment of autophagic stimulation and flux, we show that GLP-1 stimulated flux through autophagy. This was evident by an increase in LC3 II formation accompanied by a decrease in autophagosomal accumulation as assessed by mCherry-GFP-LC3 and p62. This is consistent with previous models of nutrient excess (43-44) but not tacrolimus-induced diabetes (45), suggesting that the underlying mechanism of autophagic dysfunction may determine the impact of GLP-1 agonists. There was no effect of exendin-4 on autophagy in the absence of GLT, in agreement with a previous study (17). siRNA knockdown of Atg5 prevented the exendin-4 induced increase in LC3 II and prevented the pro-survival effect of exendin-4, suggesting that activation of autophagy is a critical component of exendin-4 mediated cell survival, although additional pathways

impacting on cell survival cannot be excluded. Further assessment of autophagic flux showed that exendin-4 prevents the GLT-induced defects in lysosomal function. This is consistent with the protective effects of exendin-4 in tacrolimus-induced diabetes (45), highlighting the importance in restoring lysosomal function in the pro-survival effects of the drug. Through its ability to restore lysosomal function, exendin-4 also prevents LMP, and further stimulates lysosome biogenesis. Restoration of lysosomal function accompanied by activation of autophagy will promote removal of the accumulated autophagosomes and lysosomes, thus improving cell survival. Given that the GLT-induced increase in ER stress mediates lysosomal dysfunction in our β-cell model, it is likely that the resolution of ER stress by exendin-4, leads to an improvement in lysosomal function, and accordingly restoration of autophagic flux.

In conclusion, the results of our study show that lysosomal dysfunction mediates the loss of β-cell mass in response to glucolipotoxicity. We show that treatment with the GLP-1 agonist exendin-4 can restore autophagic flux and rescue lysosomal function. These findings support exploration of a potential therapeutic role for autophagy and lysosomal modulation for the treatment and / or prevention of type 2 diabetes and also for the further elucidation of the GLP-1 signalling mechanisms impacting on this pathway.

Acknowledgements

This work is funded by project grants from Diabetes UK (12/0004544) and Diabetes Research and Wellness Foundation (SCA/OF/11/12). We thank Dr Claus Wollheim (University Medical Center, Geneva, Switzerland) for the gift of INS-1E cells and the Clinical Islet Lab, University of Alberta, Canada, and the Islet Isolation Unit, Kings College

London, UK for provision of the human islets. We also thank Dr Helen Marshall (Institute of Cellular Medicine, Newcastle University) for her technical assistance with the rodent islet isolations and Prof Philip Home (Institute of Cellular Medicine, Newcastle University) for additional funding support.

Author Contributions

F.P.Z. acquired the data, performed data analysis and contributed to the writing of the manuscript; K.S.C. acquired the data and performed data analysis; M.M.H assisted with rodent islet isolation and human islet preparation; J.A.M.S. contributed to the concept and study design; P.E.L. contributed to the concept and study design and provided constructs; C.A. developed the concept and study design, performed data interpretation and wrote the manuscript.

C.A. is the guarantor of this work and, as such, had full access to all the data in the study and takes responsibility for the integrity of the data and the accuracy of the data analysis.

Duality of Interest

The authors declare no potential conflicts of interest relevant to this article.

Prior Presentation

Parts of this study were presented in poster form at the 51st Annual Meeting of the European Association for the Study of Diabetes, Stockholm, 14-18 September 2015 and at the Diabetes UK Annual Professional Conference, Glasgow, 2-4 March 2016.

References

1. Efeyan A, Comb WC, Sabatini DM. Nutrient-sensing mechanisms and pathways. *Nature* 2015; 517: 302-10.
2. Maiuri MC, Zalckvar E, Kimchi A, Kroemer G. Self-eating and self-killing: crosstalk between autophagy and apoptosis. *Nat Rev Mol Cell Biol* 2007; 8: 741-52.
3. Kaur J, Debnath J. Autophagy at the crossroads of catabolism and anabolism. *Nat Rev Mol Cell Biol* 2015; 16: 461-72.
4. Stienstra R, Haim Y, Riahi Y, Netea M, Rudich A, Leibowitz G. Autophagy in adipose tissue and the beta cell: implications for obesity and diabetes. *Diabetologia* 2014; 57: 1505-16.
5. Muoio DM, Newgard CB. Mechanisms of disease: molecular and metabolic mechanisms of insulin resistance and beta-cell failure in type 2 diabetes. *Nat Rev Mol Cell Biol* 2008; 9: 193-205.
6. Butler AE, Janson J, Bonner-Weir S, Ritzel R, Rizza RA, Butler PC. Beta-cell deficit and increased beta-cell apoptosis in humans with type 2 diabetes. *Diabetes* 2003; 52: 102-10.
7. Poitout V, Amyot J, Semache M, Zarrouki B, Hagman D, Fontés G. Glucolipotoxicity of the pancreatic beta cell. *Biochim Biophys Acta* 2010; 1801: 289-98.
8. Ebato C, Uchida T, Arakawa M, Komatsu M, Ueno T, Komiya K, *et al*. Autophagy is important in islet homeostasis and compensatory increase of beta cell mass in response to high-fat diet. *Cell Metab* 2008; 8:325-32.
9 Bachar-Wikstrom E, Wikstrom JD, Ariav Y, Tirosh B, Kaiser N, Cerasi E, Leibowitz G. Stimulation of autophagy improves endoplasmic reticulum stress-induced diabetes. *Diabetes* 2013; 62: 1227-37.
10. Han D, Yang B, Olson LK, Greenstein A, Baek SH, Claycombe KJ, *et al*. Activation of autophagy through modulation of 5'-AMP-activated protein kinase protects pancreatic beta-cells from high glucose. *Biochem J* 2010; 425: 541-51.
11. Choi SE, Lee SM, Lee YJ, Li LJ, Lee SJ, Lee JH, *et al*. Protective role of autophagy in palmitate-induced INS-1 beta-cell death. *Endocrinology* 2009; 150: 126-34.
12. Komiya K, Uchida T, Ueno T, Koike M, Abe H, Hirose T, *et al*. Free fatty acids stimulate autophagy in pancreatic β-cells via JNK pathway. *Biochem Biophys Res Commun* 2010; 401: 561-7.
13. Martino L, Masini M, Novelli M, Beffy P, Bugliani M, Marselli L, *et al*. Palmitate activates autophagy in INS-1E β-cells and in isolated rat and human pancreatic islets. *PLoS One* 2012; 7:e36188.
14. Las G, Serada SB, Wikstrom JD, Twig G, Shirihai OS. Fatty acids suppress autophagic turnover in β-cells. *J Biol Chem* 2011; 286: 42534-44.
15. Cnop M, Abdulkarim B, Bottu G, Cunha DA, Igoillo-Esteve M, Masini M, *et al*. RNA sequencing identifies dysregulation of the human pancreatic islet transcriptome by the saturated fatty acid palmitate. *Diabetes* 2014; 63: 1978-93.
16. Mir SU, George NM, Zahoor L, Harms R, Guinn Z, Sarvetnick NE. Inhibition of autophagic turnover in β-cells by fatty acids and glucose leads to apoptotic cell death. *J Biol Chem* 2015; 290:6071-85.
17. Abe H, Uchida T, Hara A, Mizukami H, Komiya K, Koike M, *et al*. Exendin-4 improves β-cell function in autophagy-deficient β-cells. *Endocrinology* 2013; 154: 4512-24.
18. Masini M, Bugliani M, Lupi R, del Guerra S, Boggi U, Filipponi F, *et al*. Autophagy in human type 2 diabetes pancreatic beta cells. *Diabetologia* 2009; 52: 1083-6.
19. Holst JJ. On the physiology of GIP and GLP-1. *Horm Metab Res* 2004; 36: 747–754.
20. Lavine JA, Attie AD. Gastrointestinal hormones and the regulation of β-cell mass. *Ann. N.Y. Acad. Sci* 2010; 1212: 41–58.

21. Sharma S, Mells JE, Fu PP, Saxena NK, Anania FA. GLP-1 analogs reduce hepatocyte steatosis and improve survival by enhancing the unfolded protein response and promoting macroautophagy. *PLoS One* 2011; 6: e25269
22. Li HT, Zhao XZ, Zhang XR, Li G, Jia ZQ, Sun P, *et al*. Exendin-4 Enhances Motor Function Recovery via Promotion of Autophagy and Inhibition of Neuronal Apoptosis After Spinal Cord Injury in Rats. *Mol Neurobiol* 2016; 53: 4073-82.
23. Pachera N, Papin J, Zummo FP, Rahier J, Mast J, Meyerovich K, *et al*. Heterozygous inactivation of plasma membrane Ca(2+)-ATPase in mice increases glucose-induced insulin release and beta cell proliferation, mass and viability. *Diabetologia* 2015; 58: 2843-50.
24. White MG, Marshall HL, Rigby R, Huang GC, Amer A, Booth T, *et al*. Expression of mesenchymal and α-cell phenotypic markers in islet β-cells in recently diagnosed diabetes. *Diabetes Care* 2013; 36: 3818-20.
25. N'Diaye EN[1], Kajihara KK, Hsieh I, Morisaki H, Debnath J, Brown EJ. PLIC proteins or ubiquilins regulate autophagy-dependent cell survival during nutrient starvation. *EMBO Rep* 2009 10:173-9.
26. Jackson WT, Giddings TH, Taylor MP, Mulinyame S, Rabinovitch M, Kopito RR, Kirkegaard K. Subversion of cellular autophagosomal machinery by RNA viruses. *PLoS Biol* 2005; 3: e156.
27. Stubbs M, Aiston S, Agius L. Subcellular localization, mobility, and kinetic activity of glucokinase in glucose-responsive insulin-secreting cells. *Diabetes*. 2000 49:2048-55.
28. Arden C, Petrie JL, Tudhope SJ, Al-Oanzi Z, Claydon AJ, Beynon RJ, Towle HC, Agius L. Elevated glucose represses liver glucokinase and induces its regulatory protein to safeguard hepatic phosphate homeostasis. *Diabetes* 2011; 60: 3110-20.
29. Suzuki K, Bose P, Leong-Quong RY, Fujita DJ, Riabowol K. REAP: A two minute cell fractionation method. *BMC Res Notes* 2010; 3: 294.
30. Marques C, Oliveira CS, Alves S, Chaves SR, Coutinho OP, Côrte-Real M, Preto A. Acetate-induced apoptosis in colorectal carcinoma cells involves lysosomal membrane permeabilization and cathepsin D release. *Cell Death Dis* 2013; 4:e507.
31. Klionsky DJ, Abdelmohsen K, Abe A, Abedin MJ, Abeliovich H, Acevedo Arozena A, *et al*. Guidelines for the use and interpretation of assays for monitoring autophagy (3rd edition). *Autophagy* 2016; 12: 1-222.
32. Kimura S, Noda T, Yoshimori T. Dissection of the autophagosome maturation process by a novel reporter protein, tandem fluorescent-tagged LC3. *Autophagy* 2007; 3:452-60.
33. Sardiello M, Palmieri M, di Ronza A, Medina DL, Valenza M, Gennarino VA, *et al*. A gene network regulating lysosomal biogenesis and function. *Science* 2009; 325:473-7.
34. Napolitano G, Ballabio A. TFEB at a glance. *J Cell Sci* 2016; 129: 2475-81.
35. Aits S, Jäättelä M. Lysosomal cell death at a glance. *J Cell Sci* 2013; 126: 1905-12.
36. Eizirik DL, Cardozo AK, Cnop M. The role for endoplasmic reticulum stress in diabetes mellitus. *Endocr Rev* 2008; 29:42–61.
37. Cunha DA, Ladrière L, Ortis F, Igoillo-Esteve M, Gurzov EN, Lupi R, *et al*. Glucagon-like peptide-1 agonists protect pancreatic beta-cells from lipotoxic endoplasmic reticulum stress through upregulation of BiP and JunB. *Diabetes* 2009; 58: 2851-62.
38. Yusta B, Baggio LL, Estall JL, Koehler JA, Holland DP, Li H, *et al*. GLP-1 receptor activation improves beta cell function and survival following induction of endoplasmic reticulum stress. *Cell Metab* 2006; 4: 391-406.
39. Chen YY, Sun LQ, Wang BA, Zou XM, Mu YM, Lu JM. Palmitate induces autophagy in pancreatic β-cells via endoplasmic reticulum stress and its downstream JNK pathway. *Int J Mol Med* 2013; 32: 1401-6.

40. Salehi A, Henningsson R, Mosén H, Ostenson CG, Efendic S, Lundquist I. Dysfunction of the islet lysosomal system conveys impairment of glucose-induced insulin release in the diabetic GK rat. *Endocrinology* 1999; 140: 3045-53.
41. Liu WJ, Shen TT, Chen RH, Wu HL, Wang YJ, Deng JK, *et al*. Autophagy-Lysosome Pathway in Renal Tubular Epithelial Cells Is Disrupted by Advanced Glycation End Products in Diabetic Nephropathy. *J Biol Chem* 2015; 290: 20499-510.
42. Sims-Robinson C, Bakeman A, Rosko A, Glasser R, Feldman EL. The Role of Oxidized Cholesterol in Diabetes-Induced Lysosomal Dysfunction in the Brain. *Mol Neurobiol* 2016; 53: 2287-96.
43. Liu L, Liu J, Yu X. Dipeptidyl peptidase-4 inhibitor MK-626 restores insulin secretion through enhancing autophagy in high fat diet-induced mice. *Biochem Biophys Res Commun* 2016; S0006-291: 30116-4.
44. Wang J, Wu J, Wu H, Liu X, Chen Y, Wu J, et al. Liraglutide protects pancreatic β-cells against free fatty acids in vitro and affects glucolipid metabolism in apolipoprotein E-/- mice by activating autophagy. *Mol Med Rep* 2015; 12: 4210-8.
45. Lim SW, Jin L, Jin J, Yang CW. Effect of Exendin-4 on Autophagy Clearance in Beta Cell of Rats with Tacrolimus-induced Diabetes Mellitus. *Sci Rep* 2016; 20: 29921.

Figure Legends

Figure 1. Exendin-4 increases LC3 I-II conversion in β-cells exposed to glucolipotoxicity.

A-B. INS-1E were cultured in the absence (C) or presence of 25 mmol/l glucose and 0.5 mmol/l palmitate (GLT) with or without 100 nmol/l exendin-4 (Ex-4) for 16 h. **A**. Cell death was assessed by propidium iodide (PI) - Hoechst staining and quantified as number of PI positive cells relative to total cell number. **B**. Apoptosis was assessed using the Caspase-Glo 3/7 assay.

C-E. Human islets were cultured with or without GLT / exendin-4 for 48-72 h. **C**. Viability was assessed using PI staining and quantified as percentage viability. **D-E**. Apoptosis was assessed by western blotting for cleaved caspase 3 and quantified as cleaved caspase 3 / GAPDH ratio (**D**) or using the Caspase-Glo 3/7 assay (**E**).

F-H. INS-1E (**F**), mouse (**G**) or human (**H**) islets were cultured with or without GLT / exendin-4 for either 6 h (**F**) or 48 h (**G-H**). LC3 was analysed by western blotting and quantified as LC3 II / GAPDH ratio.

N.B. Human islets consistently show higher basal LC3 II levels compared to INS-1E and mouse islets. This may be a consequence of the islet isolation procedure which places the islets under unavoidable stresses.

Results are normalised to control and expressed as fold change. Mean ± SEM of 4-6 individual experiments. *P <0.05, **P <0.01, ***P <0.005 *vs*. control; $^{\#}P < 0.05$, $^{\#\#}P < 0.01$, $^{\#\#\#}$ P < 0.005 effect of exendin-4.

Figure 2. Exendin-4 stimulates autophagic flux in β-cells exposed to glucolipotoxicity.

A. INS-1E were cultured with or without GLT / exendin-4 for 6 h. 100 µmol/l Chloroquine (CQ) was added for the final 2 h where stated. LC3 was analysed by western blotting, quantified as LC3II/GAPDH ratio and normalised to control. Open bars: Control; Light grey bars: Ex-4; Black bars: GLT; Dark grey bars: GLT + Ex-4.

B-C. INS-1E stably expressing mCherry-GFP-LC3 were either cultured in the absence or presence of 100 µmol/l chloroquine for 2h (**B**), or were cultured with or without GLT / exendin-4 for 4 h (**C**). Autophagic flux was assessed by live-cell imaging and quantified by quantification of yellow puncta using Volocity software. Results are normalised to control.

D. INS-1E were cultured on coverslips with or without GLT / exendin-4 for 16 h. Cells were fixed, immunostained for p62 and visualised using fluorescence microscopy. p62 puncta were quantified using Blobfinder software and expressed as number of p62 puncta / cell.

E. Representative immunohistochemical staining of p62 (red) and Insulin (green) from non-diabetic patients and patients with T2DM. Nuclei are stained with Hoechst (blue). Tissue was visualised using confocal microscopy. Images are representative of 3 patients with T2D and 5 controls. The intensity of islet p62 staining was quantified in control and T2D tissue, and is expressed as p62 intensity/islet.

Mean ± SEM of 3-6 individual experiments. **P* < 0.05, ***P* <0.01, ****P* <0.005 *vs*. control; $^{\#}$ *P* < 0.05 effect of exendin-4; ^ P < 0.05, ^^ P < 0.01, ^^^ P < 0.005 effect of chloroquine. Image scale bars represent 10 µm.

Figure 3. Silencing of autophagy prevents the protective effects of Exendin-4 over cell death.

A. Live cell imaging of INS-1E(mCherry-GFP-LC3) exposed to 25 mmol/l glucose and 0.5 mmol/l palmitate (GLT) for 0-24 h. Images are representative of 3 individual experiments.

B-D. INS-1E were transfected with scrambled siRNA or siRNA against Atg5 for 48 h before treatment with or without GLT / exendin-4 for 6 h (**B, C**) or 16 h (**D**). **B**. Western blotting for Atg5 and LC3 showing knockdown of Atg5. **C**. LC3 was analysed by western blotting and quantified as LC3 II/GAPDH ratio. **D**. Cell death assessed by PI/Hoechst staining. Results are normalised to control and expressed as fold change. Mean ± SEM of 4-6 individual experiments $^{*}P < 0.05$ *vs*. control; $^{\#}P < 0.05$ effect of exendin-4. Open bars: Control; Light grey bars: Ex-4; Black bars: GLT; Dark grey bars: GLT + Ex-4.

Figure 4. Exendin-4 prevents the glucolipotoxicity-induced impairment in lysosomal function.

A-D. INS-1E were cultured with or without GLT / exendin-4 for 16 h. **A**. Live cells were incubated with 75 nmol/l lysotracker red DND-99 for 30 minutes prior to fixation and visualisation with fluorescence microscopy. Puncta intensity was quantified using Blobfinder software. **B**. Lysosomes were visualized by immunostaining for Lamp2 and puncta intensity quantified using Blobfinder software. **C.** Cathepsin B activity was assessed on cell lysates using the InnoZyme Cathepsin B activity assay. **D**. Lysosomal size was determined on images from (**A**) using Image J software. Results are normalised to control and expressed as fold change.

E-F. INS-1E stably expressing GFP-LC3 were exposed to 25 mmol/l glucose and 0.5 mmol/l palmitate without or with 100 nmol/l exendin-4 for 4-8 h and lysosomes stained using 75 nmol/l lysotracker red DND-99 for the final 30 minutes. Cells were fixed and imaging using fluorescence microscopy. Images are representative of 4 experiments. Number of puncta coexpressing GFP-LC3 and lysotracker dye were quantified and expressed as yellow puncta/cell (**F**).

Mean ± SEM of 3-7 individual experiments *P < 0.05, **P <0.01, ***P <0.005 *vs*. control; $^{\#}$ P < 0.05, effect of exendin-4. Image scale bars represent 10 µm.

Figure 5. Glucolipotoxicity induces TFEB translocation and increases gene expression of TFEB targets.

A-D. INS-1E cells were cultured with or without GLT / exendin-4 for 8 h. **A**. Following fixation, immunostaining was performed for endogenous TFEB and cells visualized by fluorescence microscopy. Images are representative of 3 experiments. **B**. TFEB immunostaining was quantified via Nuclear:Cytoplasmic (N/C ratio) using Image J software. **C**. INS-1E cells were fractionated into nuclear and cytoplasmic compartments and TFEB localisation determined using western blotting for TFEB with GAPDH and Lamin A/C used as cytoplasmic and nuclear markers, respectively. Nuclear translocation was analysed using densitometry and quantified as TFEB / Lamin A/C ratio. **D**. mRNA levels of TFEB, MCOLN1, BECN1 and UVRAG were determined using RT-PCR and are normalised to control. Open bars: Control; Light grey bars: Ex-4; Black bars: GLT; Dark grey bars: GLT + Ex-4.

Mean ± SEM of 3-5 individual experiments. *P < 0.05, **P <0.01, ***P <0.005 *vs*. control; $^{\#}$ P < 0.05 effect of exendin-4. Image scale bars represent 10 µm.

Figure 6. Glucolipotoxicity-induced cell death is mediated by lysosomal membrane permeabilisation.

A, B. INS-1E were cultured with or without GLT / exendin-4 for 16 h. Following fixation, immunostaining was performed for Cathepsin B (**A**) or Cathepsin D (**B**) and cells visualized by fluorescence microscopy. Puncta intensity was quantified using Blobfinder software.

C. INS-1E were cultured in the absence or presence GLT / exendin-4 for 16 h. Lysosomal (pellet) and cytoplasmic fractions were extracted. Lysosomal membrane permeabilisation was assessed by western blotting for Cathepsin D and lysosomal and cytoplasmic fractions identified using Lamp2 and GAPDH, respectively. Cytoplasmic Cathepsin D was quantified relative to GAPDH and normalised to control.

D-F. INS-1E were pre-treated with 2.5 µl/ml antipain (**D**), 10 µmol/l CA-074 (**E**, CBi) or 10 µg/ml Pepstatin A (**F**, CDi) for 1h prior to addition of GLT for 16 h. Cell death was assessed using PI/Hoechst staining. Open bars: Control; Black bars: GLT.

G. Isolated mouse islets were cultured in the absence or presence of 25 mmol/l glucose and 0.5 mmol/l palmitate in the absence or presence of 10 µg/ml Pepstatin A (CDi) for 48 h. Caspase 3/7 activity was determined using the Caspase-Glo 3/7 assay.

H, I. Representative immunohistochemical staining of Cathepsin D (red) and Insulin (green) from non-diabetic patients and patients with T2D. Nuclei are stained with Hoechst (blue). Tissue was visualised by confocal microscopy. Images are representative of 3 patients with T2D and 5 controls. **I**. Represents higher magnification of highlighted area.

Results are normalised to control and expressed as fold change. Mean ± SEM of 3-6 individual experiments **P* < 0.05, ***P* <0.01, ****P* <0.005 *vs*. control; $^{\#}$ *P* < 0.05, effect of exendin-4; ^ P < 0.05, effect of inhibitor. Image scale bars represent 10 µm (A, B, H) or 4 µm (I).

Figure 7. The defect in lysosomal function is downstream of ER stress.

A, B. INS-1E were treated with or without 1 mmol/l 3-methyladenine (3MA) and cultured in the absence or presence of GLT / exendin-4 for 6 h (**A**) or 16 h (**B**). **A**. LC3 was analysed by western blotting, quantified as LC3II/GAPDH ratio and normalised to control. **B**. Lysosomes were stained with 75 nmol/l lysotracker red DND-99 for 30 minutes prior to fixation and

visualisation with fluorescence microscopy. Puncta intensity was quantified using Blobfinder software and normalised to control.

C-D. INS-1E were treated in the absence or presence of GLT for 4, 6 or 16 h. ER stress was assessed by western blotting for P-eIF2α (**C**) and CHOP (**D**) and quantified relative to total eIF2α or GAPDH as stated.

E-H. INS-1E were treated with or without 200 µmol/l tauroursodeoxycholic acid (TUDCA) and cultured in the absence or presence GLT / exendin-4 for 6 h (**F**) or 16 h (**E, G, H**). **E**. P-eIF2A was analysed by western blotting. **F**. LC3 was analysed by western blotting. **G**. Staining of lysosomes with lysotracker red DND-99 and quantification of puncta intensity using Blobfinder software and results normalised to control. **H**. Cell death assessed by PI/Hoechst staining and results normalised to control.

I. INS-1E were treated with or without GLT / exendin-4 for 16 h. ER stress was assessed by western blotting for P-eIF2α and quantified relative to total eIF2α.

J-L. INS-1E were treated with or without 10 µmol/l SP600125 and cultured in the absence or presence of GLT / exendin-4 for 6 h (**J, K**) or 16 h (**L**). **J**. LC3 and pJNK was analysed by western blotting. **K**. LC3 immunoreactivity was quantified as LC3II/GAPDH ratio and normalised to control. **L**. Lysosomes were immunostained using Cathepsin D antibody and cells visualized by fluorescence microscopy. Puncta intensity was quantified using Blobfinder software and results normalised to control.

Mean ± SEM of 4-6 individual experiments. Blots are representative of 2-6 experiments. *P < 0.05, **P <0.01 ***P<0.005 *vs*. control; $^{\#}P$ < 0.05 effect of exendin-4; ^ P < 0.05, ^^ P < 0.01 effect of inhibitor. Open bars: Control; Light grey bars: Ex-4; Black bars: GLT; Dark grey bars: GLT + Ex-4.

Figure 8. Schematic representation of model.

By increasing ER stress, glucolipotoxicity induces lysosomal dysfunction which prevents fusion of autophagosomes with lysosomes. Simultaneous activation of autophagy via JNK signalling causes blockage of autophagic flux and accumulation of lysosomes. This leads to accumulation of defective lysosomes resulting in lysosomal membrane permeabilisation (LMP) and release of Cathepsin D into the cytosol with subsequent induction of cell death. Inhibition of ER stress by co-treatment with exendin-4 improves lysosomal function, Exendin-4 also further stimulates autophagy leading to an improvement in autophagic flux and inhibition of LMP which directly contributes to the pro-survival effects of exendin-4.

Fig1

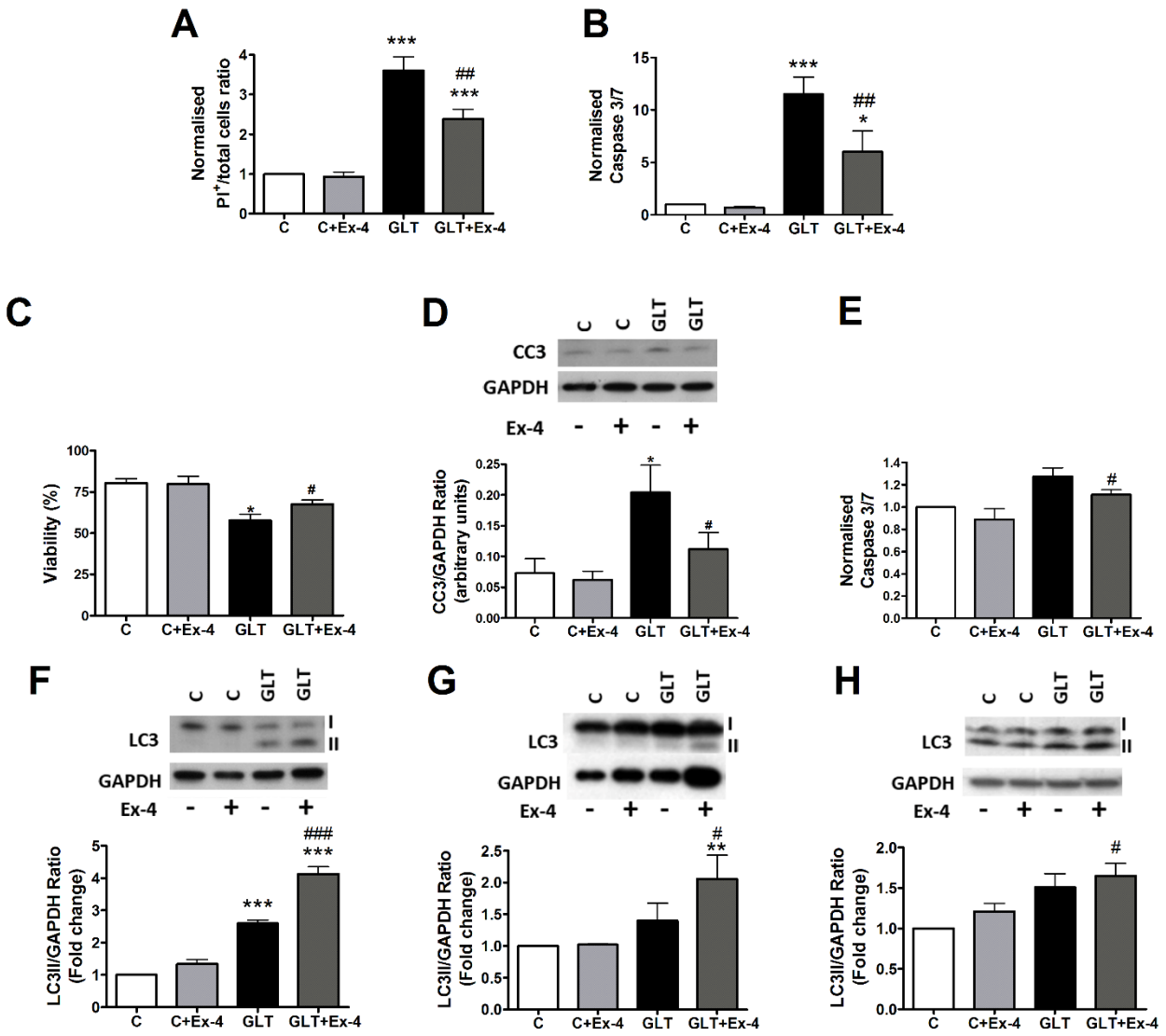
A
Normalised PI+/total cells ratio
***
##
***
C
C+Ex-4
GLT
GLT+Ex-4
B
Normalised Caspase 3/7
***
##
*
C
C+Ex-4
GLT
GLT+Ex-4
C
Viability (%)
*
#
C
C+Ex-4
GLT
GLT+Ex-4
D
C
C
GLT
GLT
CC3
GAPDH
Ex-4 - + - +
CC3/GAPDH Ratio (arbitrary units)
*
#
C
C+Ex-4
GLT
GLT+Ex-4
E
Normalised Caspase 3/7
#
C
C+Ex-4
GLT
GLT+Ex-4
F
C
C
GLT
GLT
LC3
I
II
GAPDH
Ex-4 - + - +
LC3II/GAPDH Ratio (Fold change)
###
***
***
C
C+Ex-4
GLT
GLT+Ex-4
G
C
C
GLT
GLT
LC3
I
II
GAPDH
Ex-4 - + - +
LC3II/GAPDH Ratio (Fold change)
#
**
C
C+Ex-4
GLT
GLT+Ex-4
H
C
C
GLT
GLT
LC3
I
II
GAPDH
Ex-4 - + - +
LC3II/GAPDH Ratio (Fold change)
#
C
C+Ex-4
GLT
GLT+Ex-4

Fig2

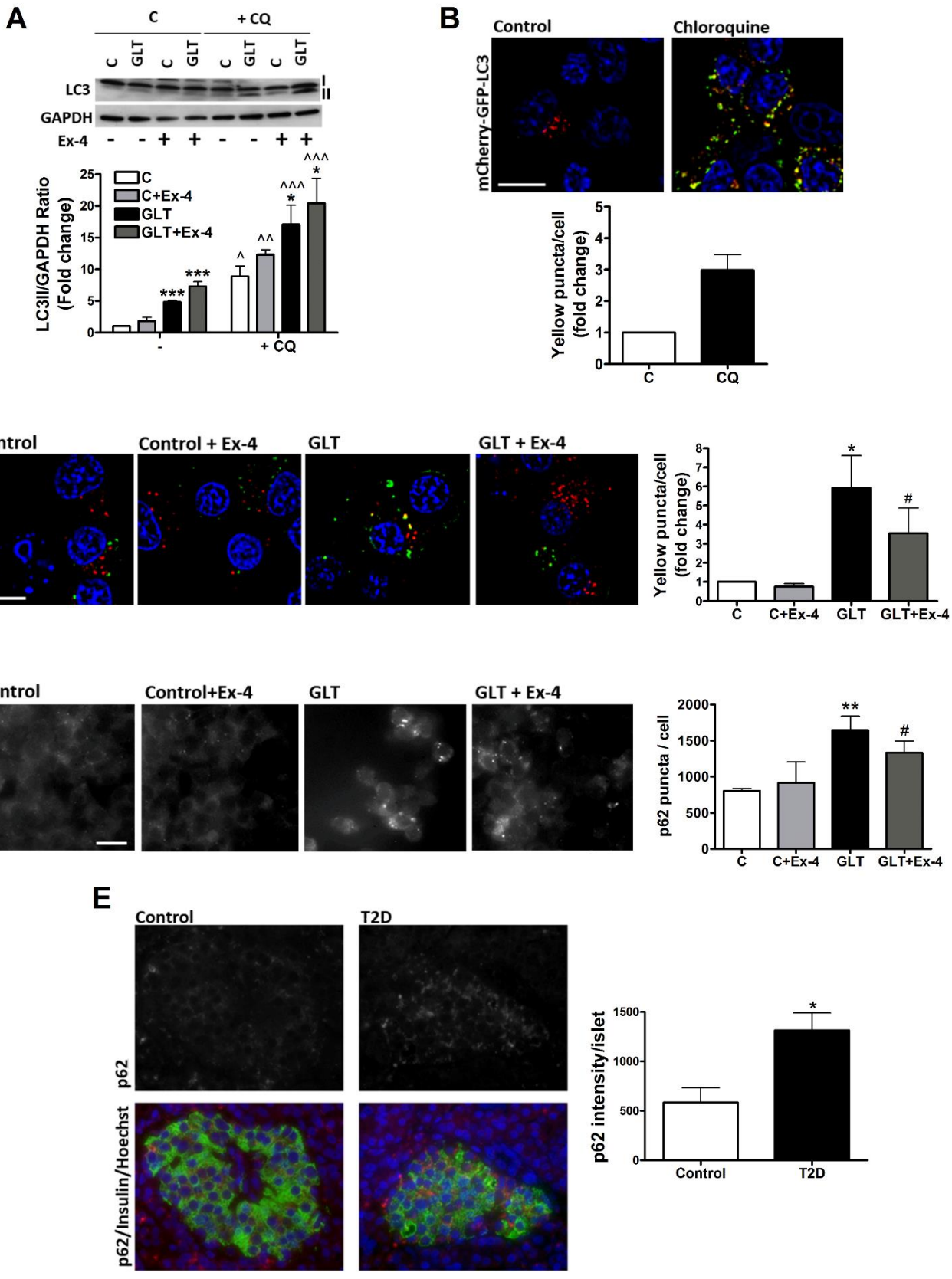
A
C
+ CQ
C
GLT
C
GLT
C
GLT
C
GLT
LC3
I
II
GAPDH
Ex-4 - - + + - - + +
LC3II/GAPDH Ratio (Fold change)
C
C+Ex-4
GLT
GLT+Ex-4
- + CQ
B
Control
Chloroquine
mCherry-GFP-LC3
Yellow puncta/cell (fold change)
C
CQ
C
Control
Control + Ex-4
GLT
GLT + Ex-4
mCherry-GFP-LC3
Yellow puncta/cell (fold change)
C
C+Ex-4
GLT
GLT+Ex-4
D
Control
Control+Ex-4
GLT
GLT + Ex-4
p62
p62 puncta / cell
C
C+Ex-4
GLT
GLT+Ex-4
E
Control
T2D
p62
p62/Insulin/Hoechst
p62 intensity/islet
Control
T2D

Fig3

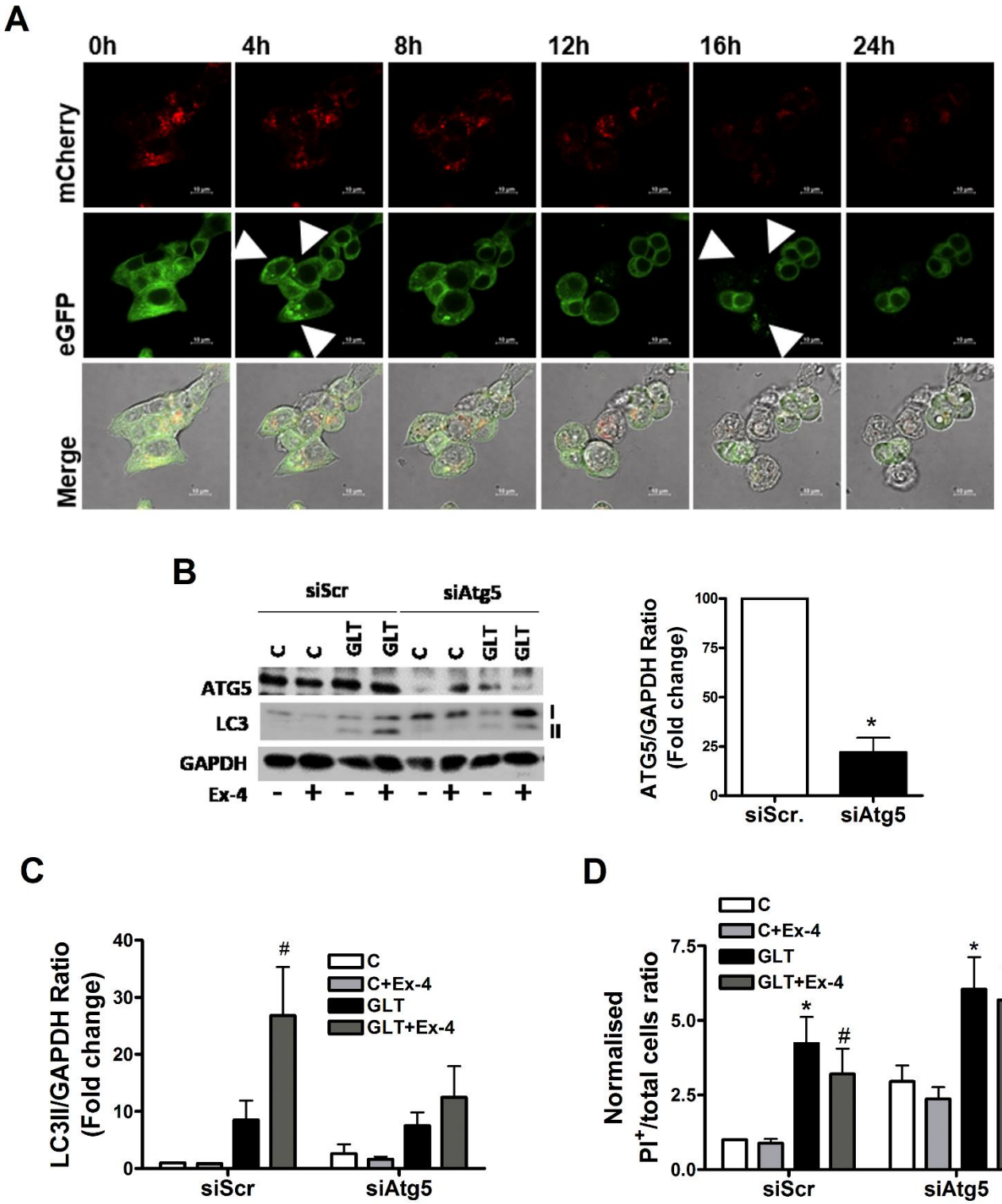
A
0h
4h
8h
12h
16h
24h
mCherry
eGFP
Merge
B
siScr
siAtg5
C
C
GLT
GLT
C
C
GLT
GLT
ATG5
LC3
I
II
GAPDH
Ex-4
- + - + - + - +
ATG5/GAPDH Ratio (Fold change)
100
75
50
25
0
*
siScr.
siAtg5
C
LC3II/GAPDH Ratio (Fold change)
40
30
20
10
0
#
C
C+Ex-4
GLT
GLT+Ex-4
siScr
siAtg5
D
Normalised PI+/total cells ratio
7.5
5.0
2.5
0.0
*
#
*
C
C+Ex-4
GLT
GLT+Ex-4
siScr
siAtg5

Fig4

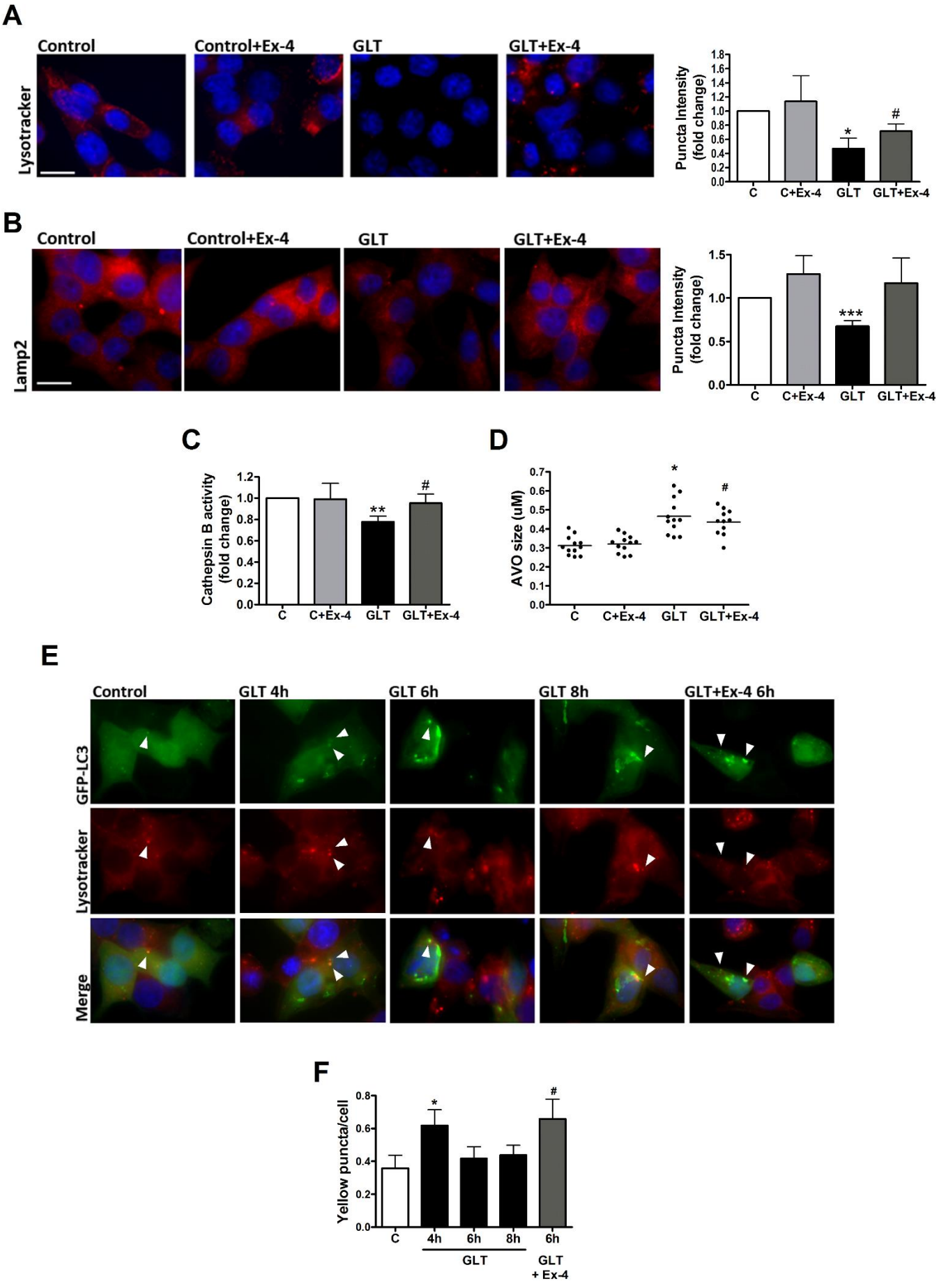
A
Control
Control+Ex-4
GLT
GLT+Ex-4
Lysotracker
Puncta Intensity (fold change)
C
C+Ex-4
GLT
GLT+Ex-4
B
Lamp2
C
Cathepsin B activity (fold change)
D
AVO size (uM)
E
Control
GLT 4h
GLT 6h
GLT 8h
GLT+Ex-4 6h
GFP-LC3
Lysotracker
Merge
F
Yellow puncta/cell
4h
6h
8h
GLT
GLT + Ex-4

Fig5

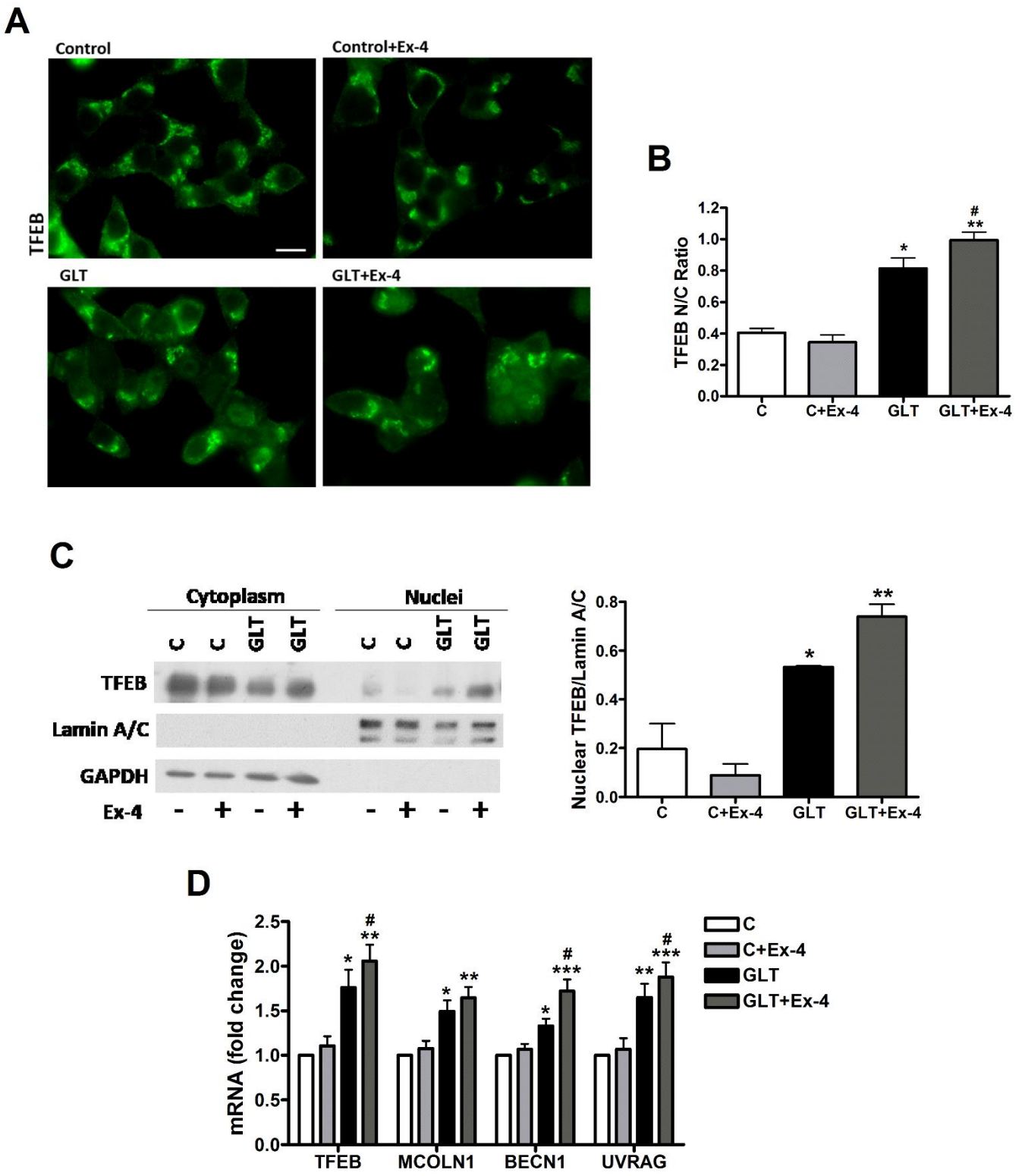
A
Control
Control+Ex-4
GLT
GLT+Ex-4
TFEB
B
TFEB N/C Ratio
1.2
1.0
0.8
0.6
0.4
0.2
0.0
C
C+Ex-4
GLT
GLT+Ex-4
C
Cytoplasm
Nuclei
C
C
GLT
GLT
TFEB
Lamin A/C
GAPDH
Ex-4
- + - + - + - +
Nuclear TFEB/Lamin A/C
0.8
0.6
0.4
0.2
0.0
D
mRNA (fold change)
2.5
2.0
1.5
1.0
0.5
0.0
TFEB
MCOLN1
BECN1
UVRAG
C
C+Ex-4
GLT
GLT+Ex-4

Fig6

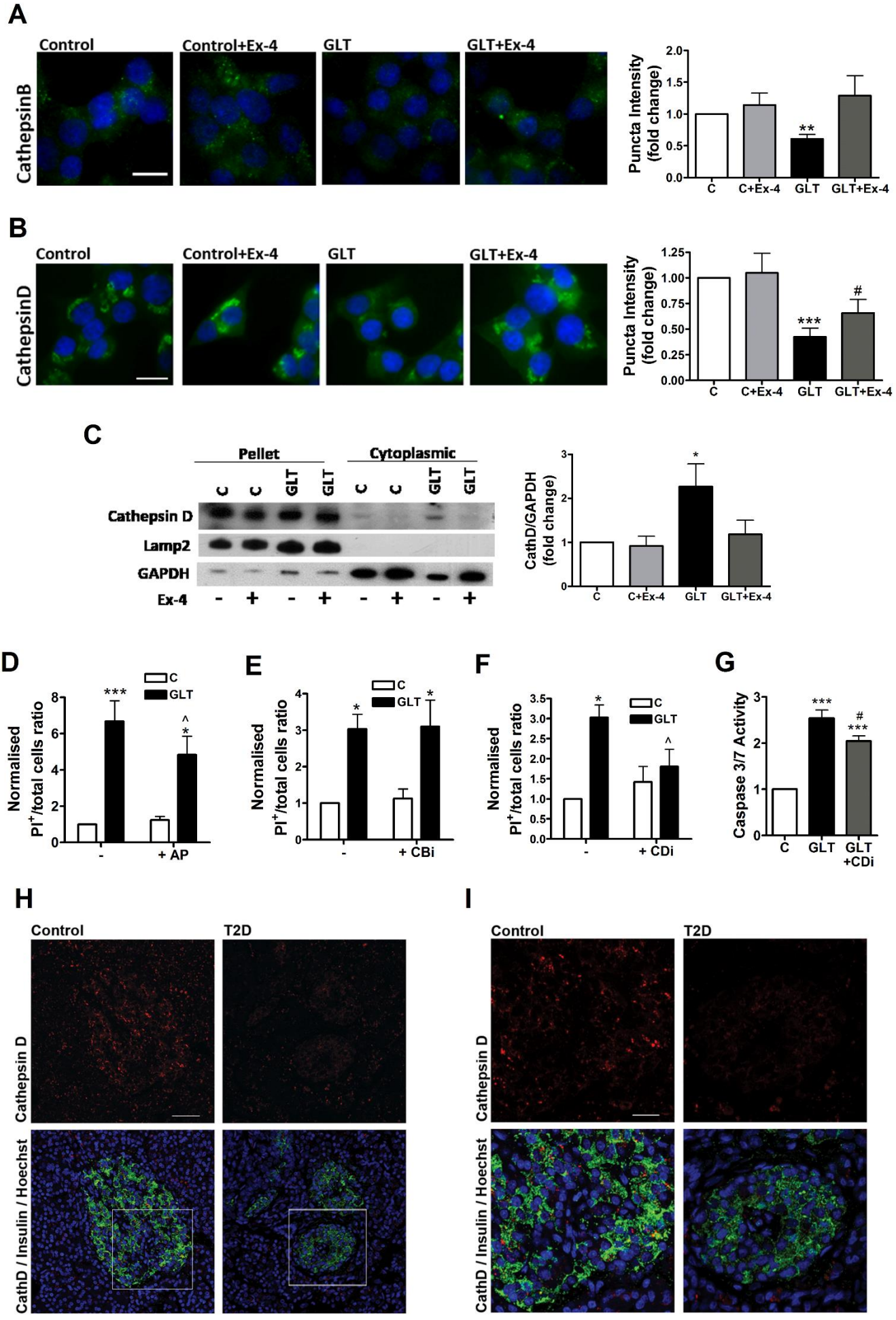
A
Control
Control+Ex-4
GLT
GLT+Ex-4
CathepsinB
Puncta Intensity (fold change)
C
C+Ex-4
GLT
GLT+Ex-4
B
CathepsinD
C
Pellet
Cytoplasmic
Cathepsin D
Lamp2
GAPDH
Ex-4
CathD/GAPDH (fold change)
D
Normalised PI+/total cells ratio
+ AP
E
+ CBi
F
+ CDi
G
Caspase 3/7 Activity
GLT +CDi
H
T2D
CathD / Insulin / Hoechst
I

Fig7

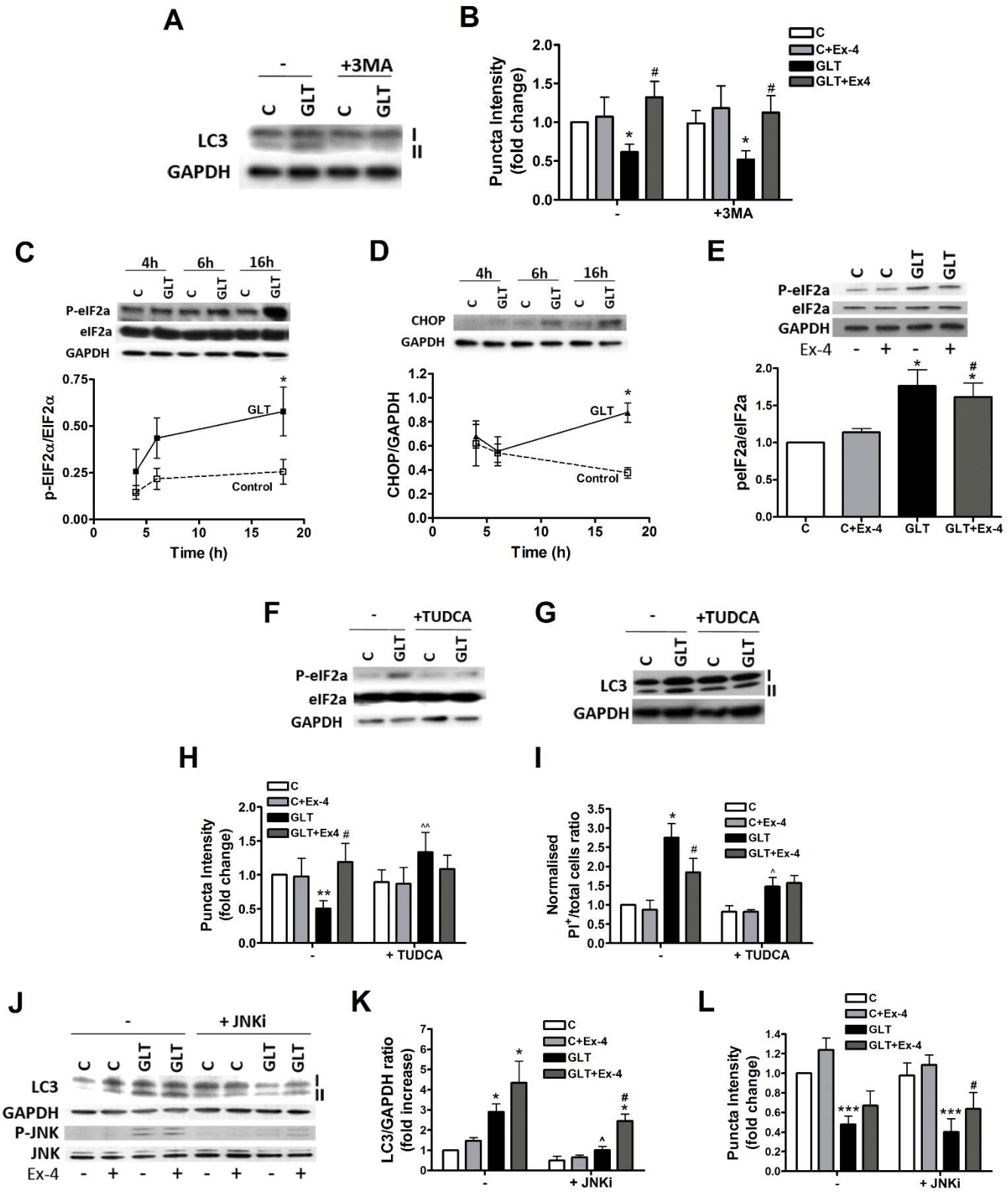
A
-
+3MA
C
GLT
C
GLT
LC3
I
II
GAPDH
B
Puncta Intensity (fold change)
C
C+Ex-4
GLT
GLT+Ex4
-
+3MA
C
4h
6h
16h
C
GLT
P-eIF2a
eIF2a
GAPDH
p-EIF2α/EIF2α
GLT
Control
Time (h)
D
CHOP
GAPDH
CHOP/GAPDH
GLT
Control
Time (h)
E
P-eIF2a
eIF2a
GAPDH
Ex-4
peIF2a/eIF2a
C
C+Ex-4
GLT
GLT+Ex-4
F
+TUDCA
P-eIF2a
eIF2a
GAPDH
G
+TUDCA
LC3
GAPDH
H
Puncta Intensity (fold change)
+ TUDCA
I
Normalised PI+/total cells ratio
+ TUDCA
J
+ JNKi
LC3
GAPDH
P-JNK
JNK
Ex-4
K
LC3/GAPDH ratio (fold increase)
+ JNKi
L
Puncta Intensity (fold change)
+ JNKi

Fig8

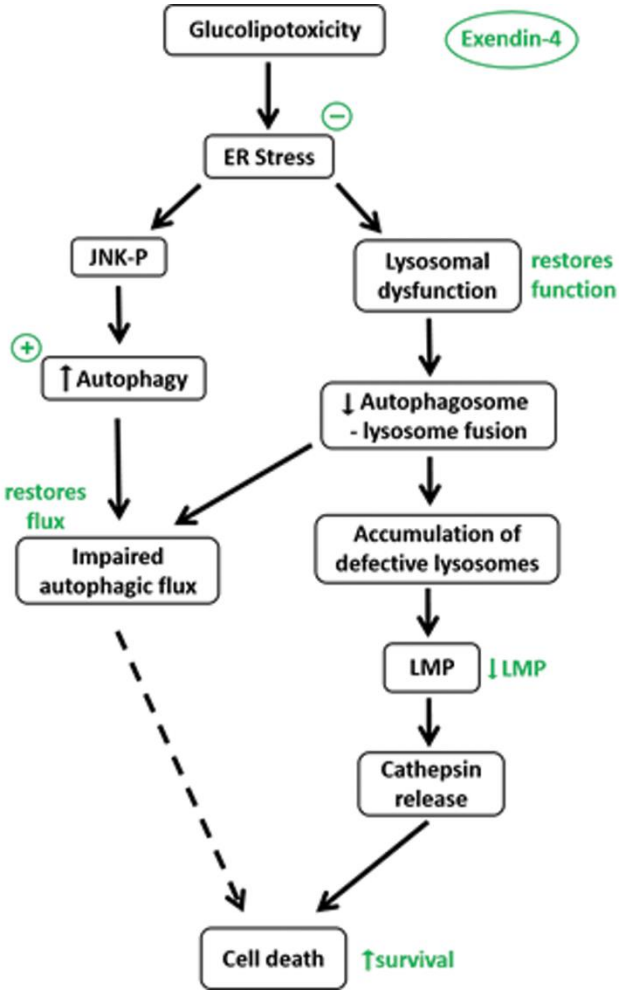
Glucolipotoxicity
Exendin-4
ER Stress
JNK-P
Lysosomal dysfunction
restores function
↑Autophagy
↓Autophagosome - lysosome fusion
restores flux
Impaired autophagic flux
Accumulation of defective lysosomes
LMP
↓LMP
Cathepsin release
Cell death
↑survival

Supplementary Video 1

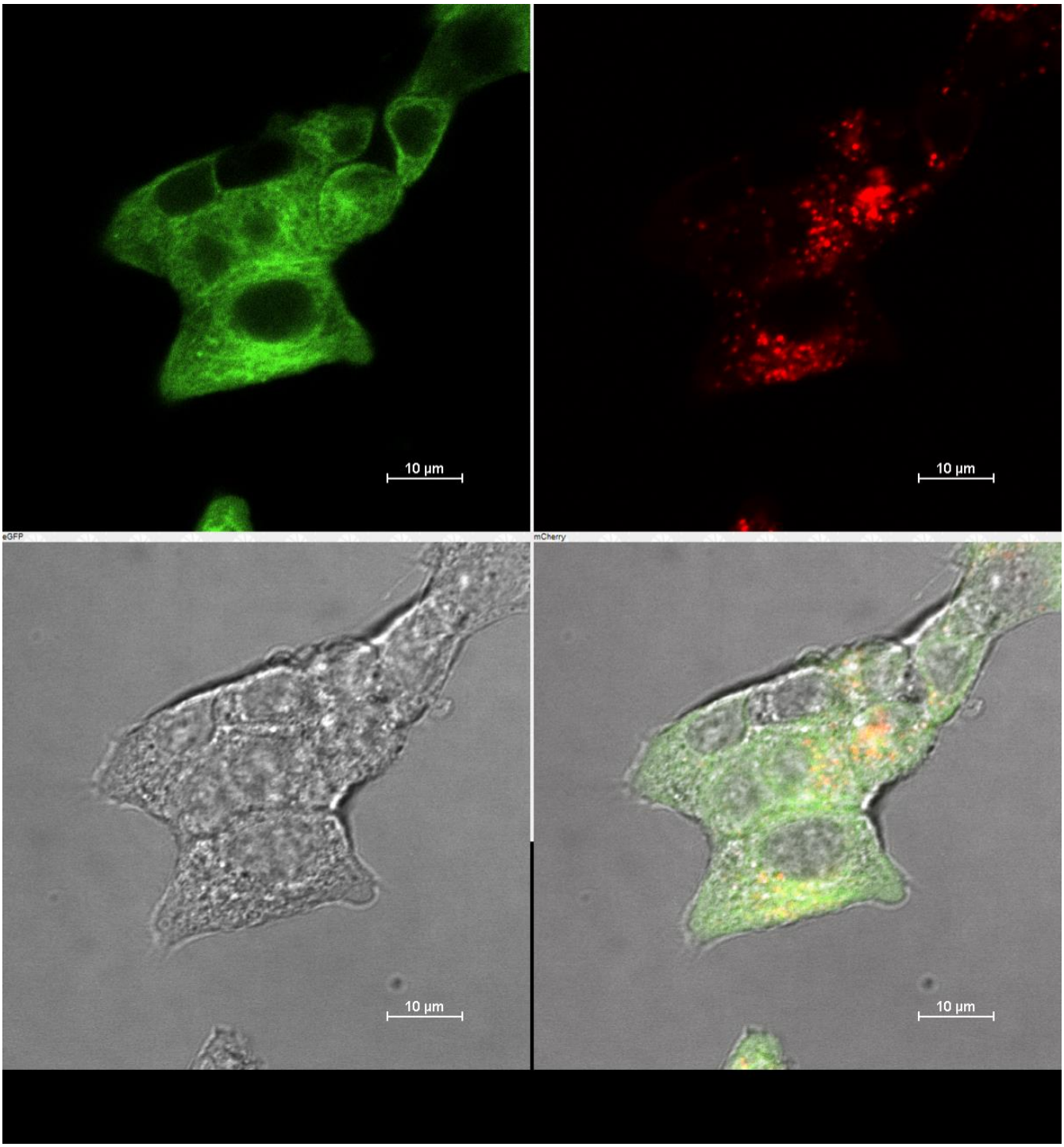

Supplementary Fig1

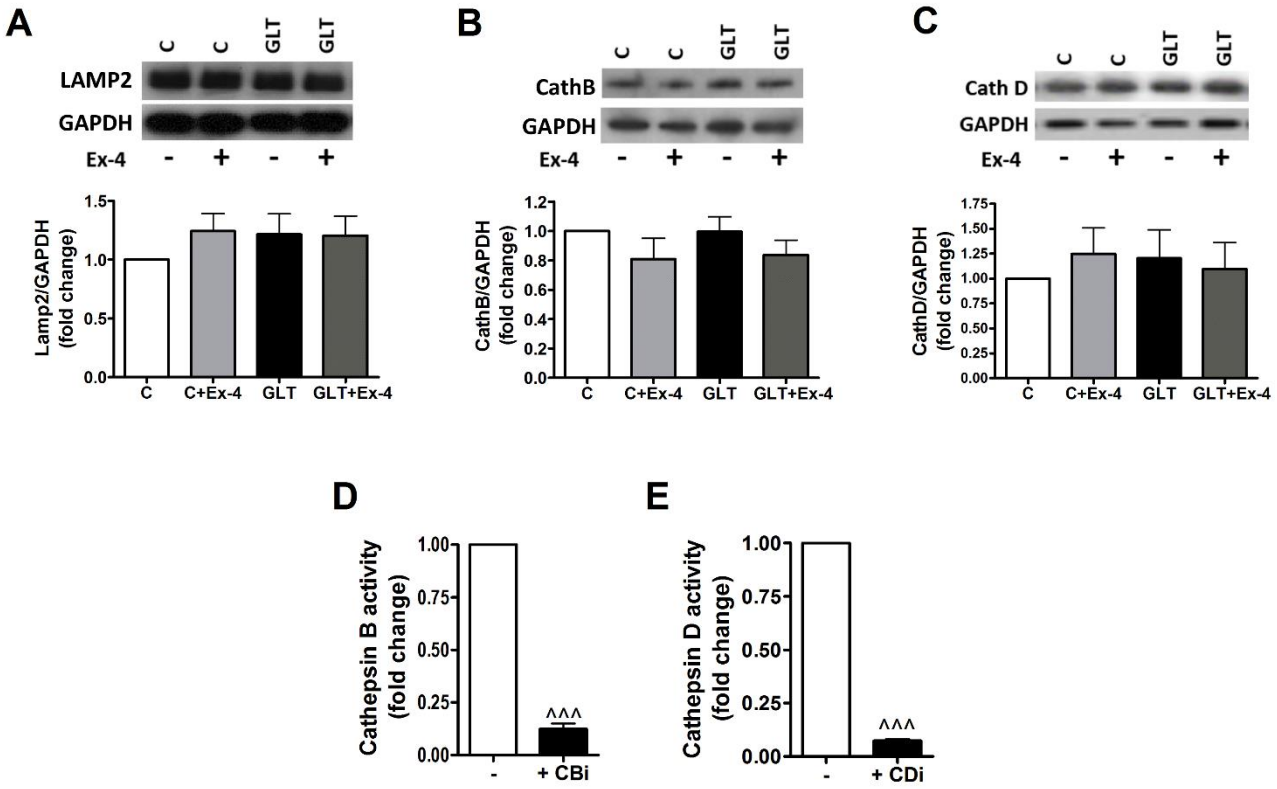

Supplementary Figure 2

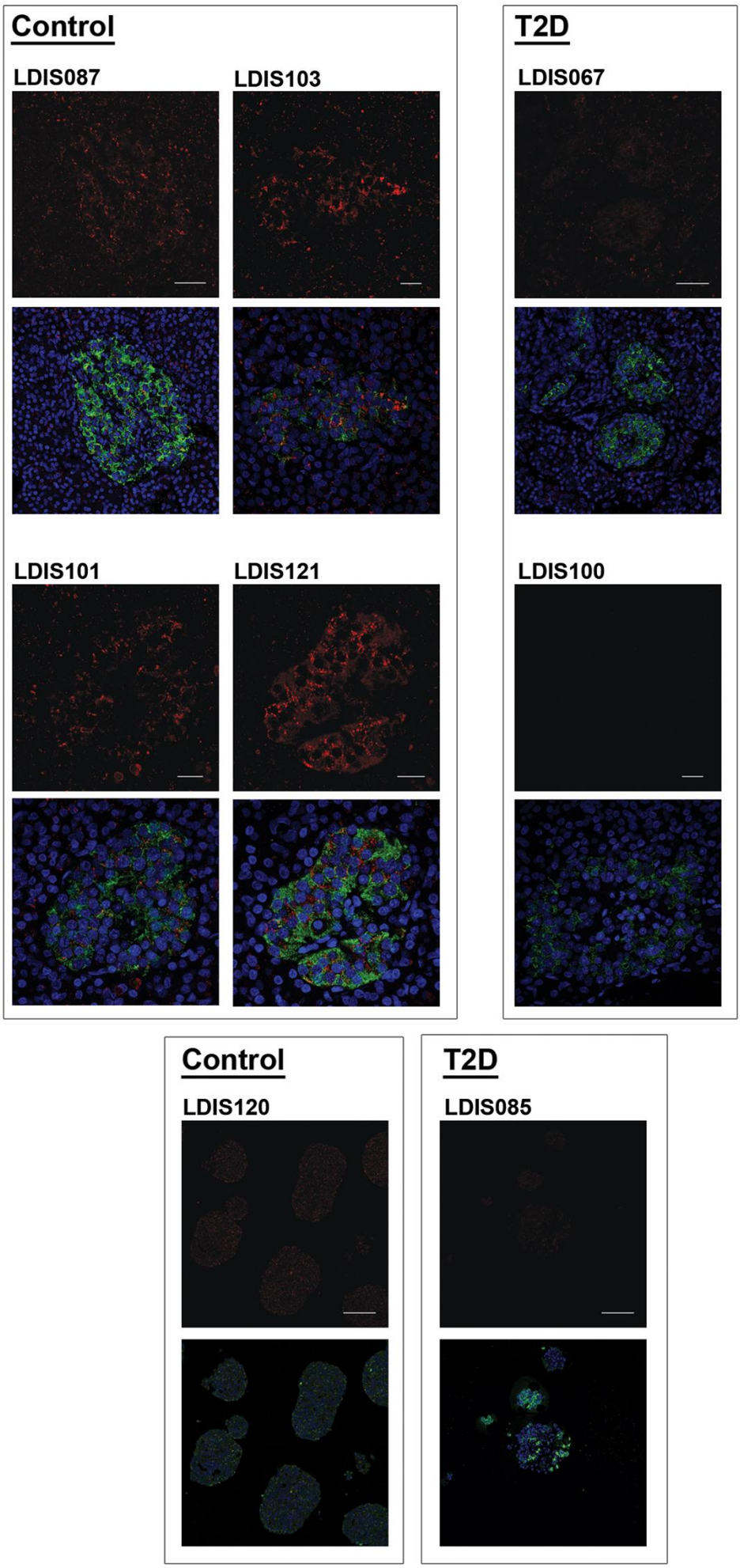

Online Supplemental material

Table S1. Antibody details

Target	Catalogue number	Company
ATG5	NB110-53818	Novus Biologicals
Cathepsin B	06-480	Merck Millipore
Cathepsin D	SC-6487	Santa Cruz
CHOP	SC-575	Santa Cruz
Cleaved Caspase 3	9661S	Cell Signaling Technology
p-eIF2α	3398P	Cell Signaling Technology
Total eIF2α	5324P	Cell Signaling Technology
GAPDH	5G4	Hytest
Insulin	A0564	Dako
Insulin	I2018	Sigms Aldrich
p-JNK	4668T	Cell Signaling Technology
Total JNK	SC-474	Santa Cruz
Lamin A/C	2032S	Cell Signaling Technology
LAMP2	L0668	Sigma Aldrich
LC3	L7543	Sigma Aldrich
p62	GP62-C	Progen
TFEB	A303	Bethyl Laboratories

Table S2. Primer sequences for real-time RT-PCR

Gene	FWD	REV
TFEB	CTG GAG ATG ACC AAC AAG CA	GTG AGG TGG TGG GAA GAC C
MCOLN1	GGC GCC TAC GAC ACT ATC A,	TAG GCC TGG AGC TCA CTC TT
BECN1	CAG GCG AAA CCA GGA GAG	CGA GTT TCA ATA AAT GGC TCC T
UVRAG	GGA AAG ACA GAA GAA AGC TCT GG	CGG CAA ATG CAC TTC CTT
Cyclophilin A	ATG GCA CTG GTG GCA AGT CC	TTG CCA TTC CTG GAC CCA AA

Supplementary Figure 1

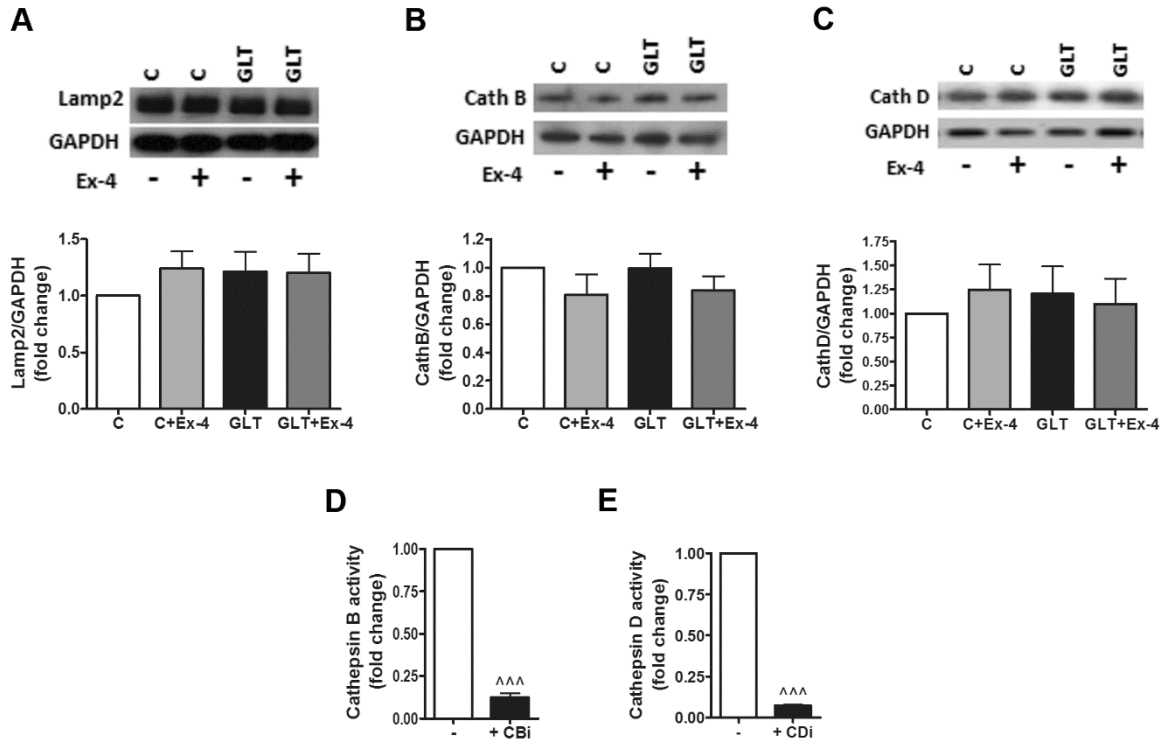

Figure S1. Cathepsin expression and inhibition of Cathepsin activity in beta-cells.

A-C. INS-1E were cultured in the absence or presence of 25 mmol/l glucose and 0.5 mmol/l palmitate with or without 100 nmol/l exendin-4 for 16 h. Lamp2 protein (**A**), cathepsin B (**B**) and cathepsin D (**C**) expression was assessed by western blotting and quantified relative to GAPDH.

D-E. INS-1E were treated with 10 µmol/l CA-074 (**C**, CBi) or 10 µg/ml Pepstatin A (**D**, CDi) for 16 h. Cathepsin B and D activity was determined on cell lysates using the InnoZyme Cathepsin B activity assay and RayBio Cathepsin D activity assay, respectively.

Results are normalised to control and expressed as fold change. Mean ± SEM of 3-6 individual experiments. ^^^ $P < 0.005$, effect of cathepsin inhibitor.

Supplementary Figure 2

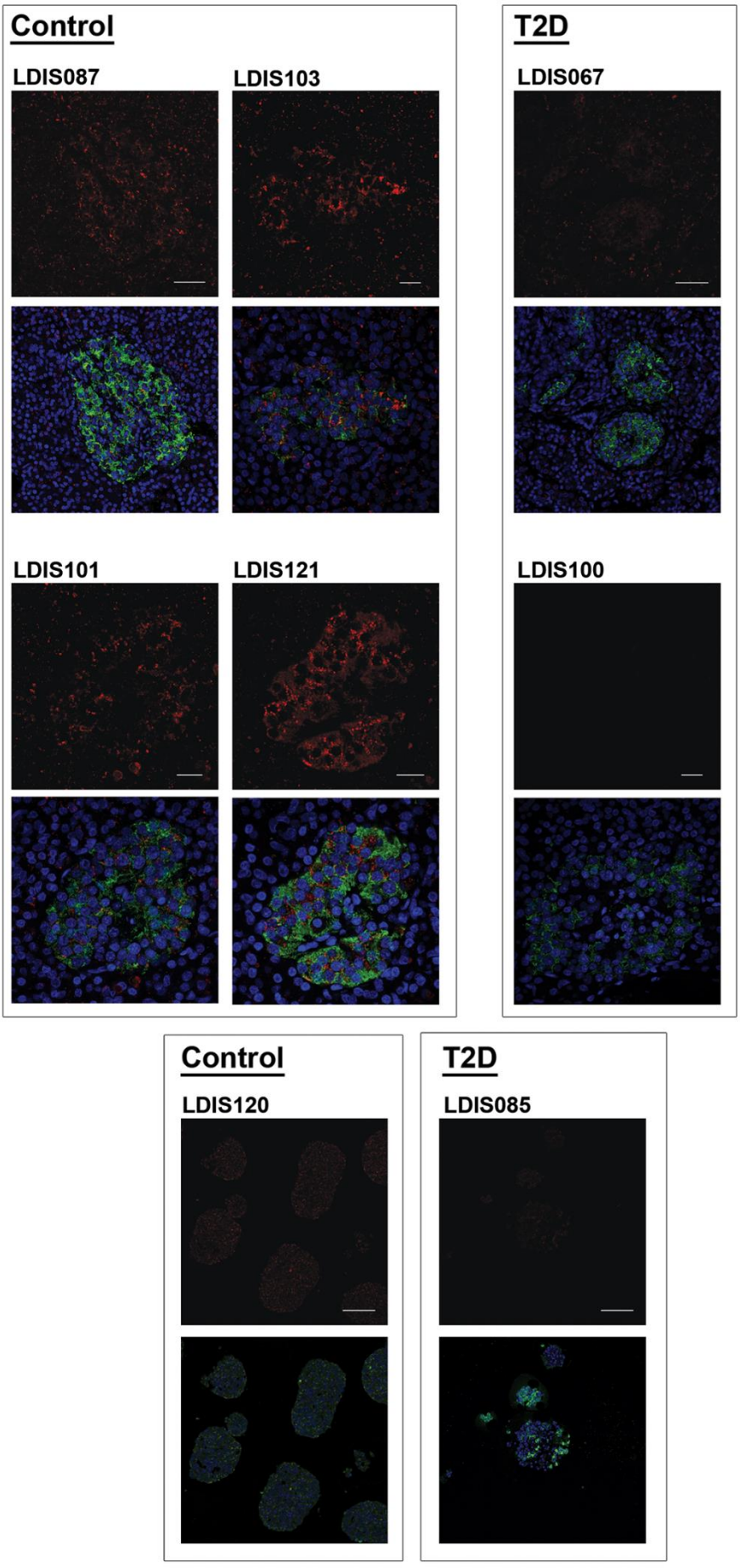

Figure S2. Cathepsin D immunohistochemical staining in T2DM

Immunohistochemical staining of Cathepsin D (red) and Insulin (green) from non-diabetic patients and patients with T2DM. Nuclei are stained with Hoechst (blue). Tissue was visualised using confocal microscopy. Tissue sample from control patients; n = 5; T2DM patients, n = 2; Embedded islets from control patients; n = 1; T2DM patients, n = 1. 3 islet-containing images were taken for each patient and representative images for each patient are shown.

Video S1. Live-cell imaging of autophagic flux

INS-1E(mCherry-GFP-LC3) were exposed to 25 mmol/l glucose and 0.5 mmol/l palmitate and live-cell imaging performed for 0-24 h. Video is representative of 3 experiments.